DESTination RAIL – Decision Support Tool for Rail Infrastructure Managers
Project Reference: 636285
H2020-MG 2014-2015
Innovations and Networks Executive Agency
Project Duration: 1 May 2015–31 April 2018

Deliverable 1.3
Report on monitoring Switches and Crossings

Authors
*** Elias Kassa (NTNU), Jan Sramota (NTNU), Amir Kaynia (NGI)**

*Corresponding author: Elias Kassa, elias.kassa@ntnu.no

Date: 12/10/17
Dissemination level: (PU, PP, RE, CO): PU
This project has received funding from the European Union's

This project is funded by the European Union

DOCUMENT HISTORY

Number	Date	Author(s)	Comments
01	19/10/2017	Elias Kassa	First draft of the document was sent to Amir Kaynia (NGI) for review
02	20/10/2017	Amir Kaynia	Amir Kaynia returned the document with comments
03	24/10/2017	Elias Kassa	Final report complete
04	18/11/2017	Elias Kassa	Minor revision

Table of Contents

1 Executive Summary 4
2 Introduction 5
3 Dynamic modelling 7
3.1 Vehicle-track-substructure modelling 7
3.2 Rail acceleration sampling locations 12
3.3 Rail acceleration sensitivity 13
3.4 Summary 17
4 Instrumentation 17
4.1 Background 17
4.2 System architecture 18
4.3 Wireless sensor hardware platform 19
4.4 Power consumption of wireless sensor 27
4.5 Transmission and communication network 28
5 System evaluation and validation 33
5.1 Test of concept feasibility 33
5.2 Antenna test 34
5.3 Rail coverage test 35
5.4 Field tests 36
6 Conclusions 47
7 References 49
Appendix A: Schematic 51
Appendix B: PCB Layout 52
Appendix C: Tommerup Test site 53
Appendix D: Acceleration Measurements 58
Appendix E: Desynchronization 65

1 Executive Summary

Monitoring the condition of switch and crossings is a challenge for infrastructure managers (IMs). It requires specially trained switch inspectors to manually check the condition of the track. Hence, a fast and cheap system to continuously monitor the Switches and Crossings is a crucial matter for railway IMs. Partners of this task developed a methodology for continuous and real-time inspection of critical track infrastructures, such as switches and crossings, using sensor technologies. The system was successfully tested in lab environment and deployed at field test-site in Denmark and Germany.

This report summarises the work done in developing a methodology to continuously monitor Tracks and Switches and Crossings, using inbuilt sensor technologies. The architecture of the sensor network developed contains communication platform to transfer data to a remote station in real time to follow up the status and condition of the track being monitored. A train-track interaction simulation tool was developed to select suitable sensors architecture and communication, and to identify optimum sensor location along the track.

The partner NTNU has developed the sensor network and storage system, and communication system to transfer data in real time. The system was tested in a lab environment before the inbuilt technology was mounted in field demonstration. The system was installed in track infrastructure and the different stages and levels were tested in field. All the objective of the Task 1.3 have been achieved. The monitoring system have been installed at a railway line in Germany to compare the vibration measurements with existing and expensive measurements as a validation exercise. The system has proved to have a potential for a smart failure and fault detection in rail infrastructure at network level.

2 Introduction

Monitoring of track condition is performed by rail infrastructure managers (IMs) using instrumented trains. The instrumented trains monitor the geometric quality of the track and some IMs have a special train to inspect the track stiffness as a way of track condition monitoring. Continuous and more accurate monitoring by instrumented trains allowed the IMs to estimate the rate of track deterioration, to optimize track maintenance schedules and to replace only worn-out parts of the track. As for Switches and Crossings (S&Cs), these vehicles are not fully applicable to monitor the S&Cs. Often the inspection at S&Cs is done manually by specially trained switch inspectors to check the condition of the track. This may lead to situations where just some parts of the rail track is inspected and decision is made based on many local measurements. Due to this fact, the whole track might often be replaced before the end of the life cycle. Therefore, the same revolution as in assessment of geometric quality of the rails is now requested.

A fast and cheap system to monitor the S&Cs is a crucial matter for railway IMs. The tasks in this project aim to develop a methodology to continuously monitor tracks and switches and crossings, using inbuilt sensor technologies. The key demand of this task is to create a system, which will be fast, cheap and provide continuous monitoring on switch and crossings. Solution should be inbuilt and allow high integration into already existing infrastructure. System should provide real-time information about condition of the track to a remote maintenance centre. Communication system, data analysis and storage system should be part of the final solution. To fulfil all of this demands, that is low-costs and easy integration, decision was made in this project to use as much of the already existing railway infrastructure as possible.

In this report several sub-tasks contributing to the goal of Task 1.3 is presented. The first section is dealing with the train-track-substructure model developed by coupling a Multi Body System dynamics tool Gensys (Persson, 2009) with a Finite Element model in Abaqus (Hibbitt, et.al, 2013). The analysis has been used to identify sensor location where signals vary less with respect to different variables and that satisfy the regulations by the railway administration.

The rail acceleration is the main content of the railway dynamic test, and it is used to evaluate the vibration characteristics of track structure or wheel-rail impact effect. Remington (1987) installed six acceleration sensors across the rail between two sleepers, and measured rail acceleration to predict wheel-rail noise. Zhao and Wang (2015) measured rail vibrations in transition zone between slab and ballasted track by using acceleration sensors on top of railhead and rail foot above the sleepers.

The rail is a spatial structure that consists of railhead, rail web and rail foot, and it is supported discretely by sleepers or concrete blocks in longitudinal direction. The rail is the most important component in a railway track system and has functions of guiding

wheels, supporting wheel loads and distributing the loads over several sleepers. The structural health of the rail and the supporting structure therefore needs to be inspected and monitored continuously. Various position of the spatial rail will have different accelerations (Bracciali and Cascini, 1997).

The rail vibration acceleration can have impact on the wheel-rail contact and this can be reflected in the track condition and track quality. Hence, it is usually used as the main index for investigation of track dynamics and track condition in theoretical analysis and in field test. Field dynamic tests carried out to measure accelerations at single points, without considering the acceleration sensitive area, will have influence on the accuracy of the test results. Thus, it is important to identify acceleration sensitive areas across the rail as well as along the track under train dynamic loading.

The first section of the report discusses the modelling of a train-track-substructure dynamic system using the coupled finite element tool ABAQUS and the MBS code Gensys. The vibration analysis of the rail acceleration has been performed, considering track irregularity conditions, train speeds and contact patch location. Results of the rail acceleration under certain irregularity and different train speeds are presented to determine the feasible areas for sensor placement. The range and frequency of the rail vibration acceleration is identified and summarised in the first section of this report. The outcome from this task was used to provide guidance to field test instrumentation for monitoring of railway track condition.

The second section of the report summarises the work done on the development of the monitoring instrumentation. The methodology for continuous and real-time monitoring of switches and crossings were developed. The system is based on battery powered sensor networks and a wireless communication system. Wireless sensors containing digital accelerometer and wireless module sense the vibration from the passing train for continuous monitoring and transmitting acceleration data to the network. Each sensor has own battery, that should power the device for many years. The important aspect of the sensor is ultra-low power consumption to achieve very long lifespan. Acceleration data are sent to the gateway and passed through GSM-R or WiFi to the dedicated server. The data are aggregated, analysed and stored.

Issues connected to outdoor environment were revealed during the first field test and were addressed during the second field demonstration. Due to positive results such as very cheap cost of the wireless sensor, reliability of data sampling, storage and transfer, such a technology has a huge potential for the needs of IMs to monitor their track, and switch and crossing infrastructures.

3 Dynamic modelling

This section covers the train-track interaction dynamic system modelling to identify sensitive areas of vibration acceleration across the rail structure as well as along the track under train dynamic loading. Different factors were included in the assessment to analyse their effects on the rail acceleration. The range and frequency of the rail vibration acceleration is identified as a guide in the subsequent tasks. For further detail refer to Cai and Kassa (2016).

3.1 Vehicle-track-substructure modelling

A train-track–substructure dynamic system was modelled using Finite Element (FE) tool Abaqus and the Multi Body System (MBS) dynamics code Gensys. From the dynamic analysis of vehicle-track interaction, the time history of the contact force and contact point location is obtained. The time history data of wheel-rail force and wheel-rail contact point from Gensys simulation are used as input in the FE simulation. The accelerations of rail head, rail web and rail foot are obtained from the FE simulation.

3.1.1 Vehicle-track dynamic model

An MBS code Gensys is used for modelling the vehicle system with all the components represented in detail while the track system is represented by simple mass-spring-damper system coupled to each wheel. Gensys is a three-dimensional multi-body-dynamic program for modelling rail vehicles running on track. Gensys is widely applied in analyzing dynamic behaviour of vehicles and it enables to calculate vehicle vibration, wheel-rail force and wheel-rail contact patch, etc. The vehicle-track coupling dynamic model consists of vehicle model, track model and wheel-rail contact model.

3.1.1.1 Vehicle model

The vehicle is modelled as a multi-body system composed of a car body, two bogie frames and four wheelsets, see Figure 1. The car-body, bogie frames and wheelsets as rigid bodies are connected by suspension systems which are simulated by spring-damper elements. The connection between car body and bogie frame is simulated by spring-damper element representing the secondary suspension parameters and the link between bogie and wheelset is simulated by spring-damper element representing the primary suspension parameters. The entire vehicle model is a longitudinal-lateral-vertical space coupled system with 38 degrees of freedom.

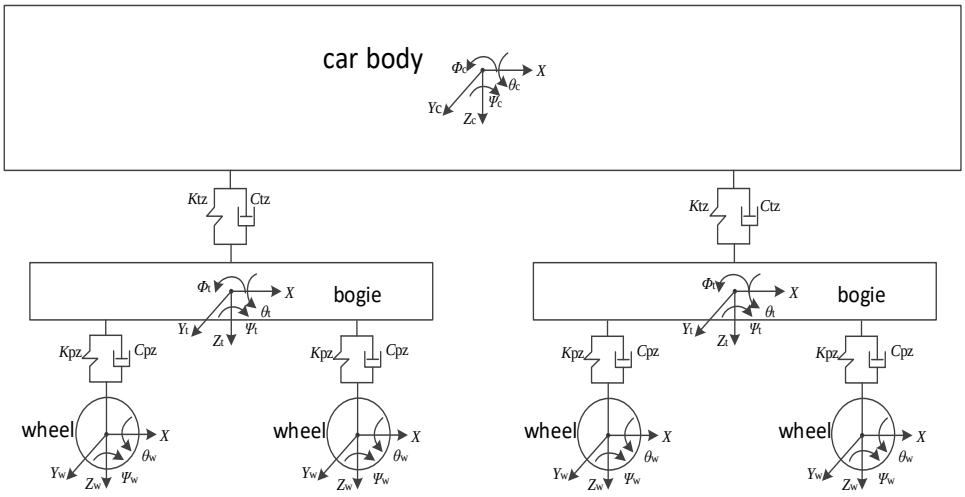

Figure 1 The vehicle model

3.1.1.2 Track-substructure model

A FE tool ABAQUS is used to model the track. The track is taken as continuous elastic support model. The rail structure is simulated by Euler beam and the support type of foundation such as ballast bed, sleeper, etc. is simulated by single continuous support model. The rail and sleeper are connected by several fasteners which can be modelled by springs with linear property and dampers with viscous property. The wheel-rail contact relationship which is tied between vehicle and track includes normal interaction and tangent interaction. The non-linear Hertz elastic contact theory is used to calculate the normal contact forces. The normal force *p(t)* is generated by the compression of the wheel and rail, and it would disappear when they separate. The force is defined as follows:

$$p(t) = \left[\frac{1}{G}\Delta Z(t)\right]^{\frac{3}{2}} \quad (1)$$

Where G is the wheel-rail contact coefficient and $\Delta z(t)$ is the normal elastic compressing deformation at wheel-rail contact patch.

The analysis of tangent interaction takes the creep ratio of the wheel-rail into account. First, Kalker creep theory FASTSIM was used for the calculation of creep forces, and then the Shen's theory was adopted in the amended results. The creep force is nonlinear which contains longitudinal and lateral forces.

For the ballasted track, the track-substructure FE model includes rail, fastener, sleeper, ballast bed and subgrade layers. The properties of the track model are given in Table 1. The fastener was simulated by spring-damper element and the ballast and the

subgrade support structural components were simulated by deformable solid structure. The rail pad at each fastener was modelled by three spring-damper elements in longitudinal and in lateral directions, which gives 9 spring-damper elements representing the rail pad and fastening system. The average stiffness is distributed equally among the nine elements. The ballast bed was simulated by C3D8R solid element in Abaqus.

Rail	
profile	UIC60
Cross-section area	76.86 cm^2
Moment of inertia horizontal axis	3055cm^4
Moment of inertia vertical axis	512.9cm^4

Ballast	
Ballasted bed thickness	0.3m

Fastening system	
Vertical stiffness	7.5×10^7N/m
Lateral stiffness	3.9×10^7N/m

Sleeper	
Concrete sleeper dimension	2.6×0.2×0.3 m

Table 1 Track model properties

The rail and the fastening system model is shown in Figure 2. The track substructure model is shown in Figure 3. To a certain extent, the track vibration is affected by foundation structure, so the vibration of the subgrade was considered in the model. The height of the subgrade in the model is 3m and the side slope is 1:1.75. In order to eliminate influence of the boundary condition from the track end condition, the length of the integral model was taken 100m and the measuring point of rail acceleration is in the centre of the model. Further, in order to prevent vibration reflection, spring-damper element as absorbing boundary was adopted in each side of the model.

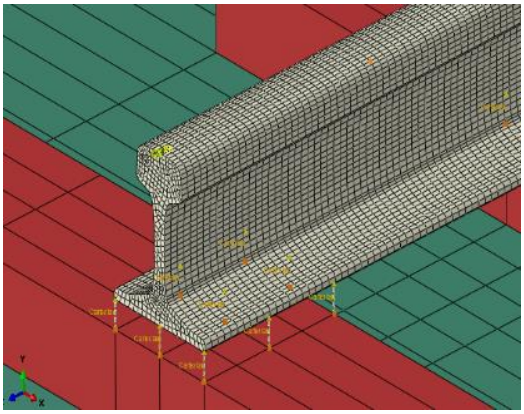

(a) 3D view of rail

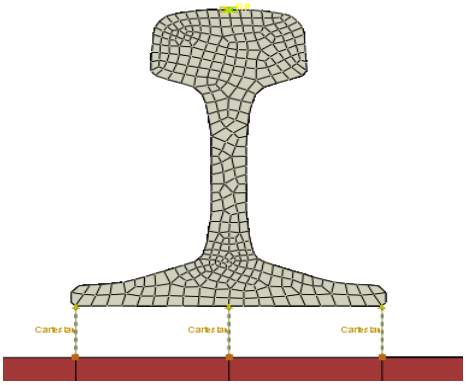

(b) front view of rail

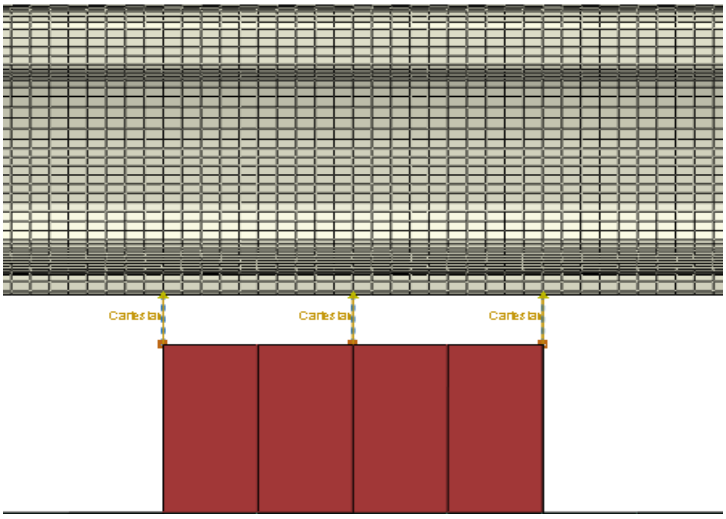

(c) lateral view of rail

Figure 2 Rail and fastening systems model

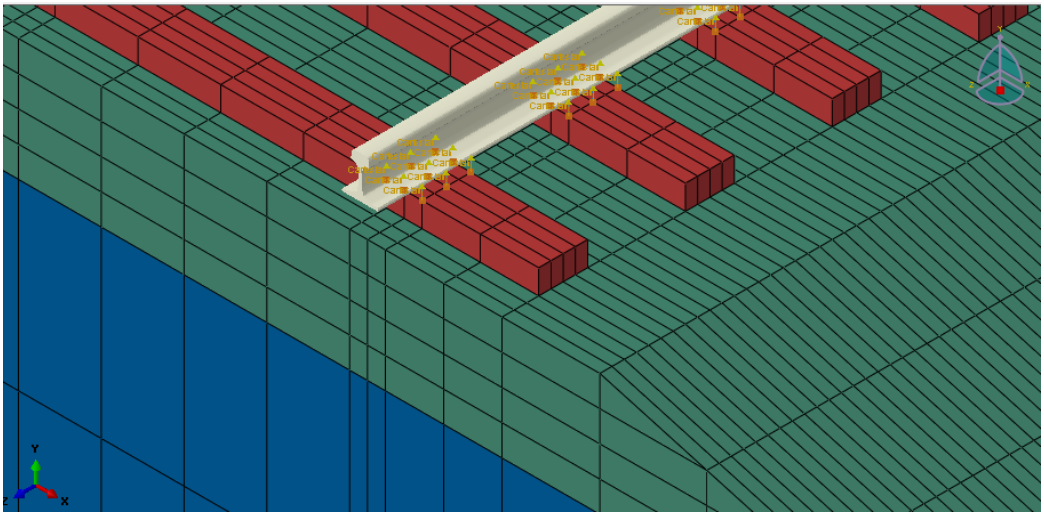

Figure 3 Track-substructure FE model

3.1.2 Wheel-rail force transfer

The dynamic interaction of a vehicle and a track is transmitted through a wheel-rail contact. The rail and wheels are considered as elastomer with very large elastic modulus. According to Hertz contact theory, the shape of the wheel-rail contact patch is elliptical, and the contact occurs on the top surface of the railhead, as is shown in Figure 4. The uneven distribution of stress in elliptical contact patch is neglected in the process of load application assuming the contact patch as a sliding load platform on the surface of the railhead.

At first the vehicle was simulated in running a straight line. The contact point trajectory predicted by the Gensys model indicated a slight lateral displacement of contact patch on the surface of railhead. However, the slight displacements of the contact trajectory was excluded for the subsequent Abaqus modelling. The dynamic interaction between wheel and rail in the model was assumed by a non-linear Hertz contact. In the model, the wheelset velocity was set as boundary conditions applying to load platform.

The wheel-rail contact force calculated by the MBS tool Gensys was used as the excitation source to FE model. The contact force is a discrete function of time and it was imported into the FE model in order to simulate real wheel-rail time history. Based on Abaqus pre-process environment, wheel-rail contact force was applied in the elliptical load platform in the FE model, which is moving with the load platform. In addition, the lateral contact force was found to be much smaller compared to the vertical contact force; threfeore, it is feasible to neglect the effect of lateral force without noticeably compromising the final result.

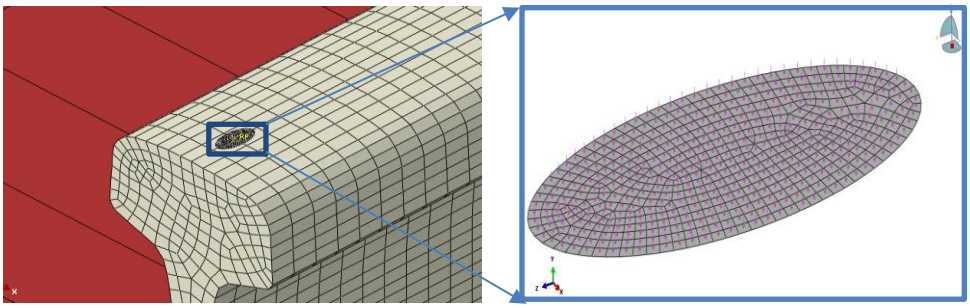

Figure 4 Elliptic shape of the wheel-rail contact load platform

3.2 Rail acceleration sampling locations

Ballasted track is the main form of the railway track, accounting for about 90% of railway in the world. In the ballasted track, the rails and concrete sleepers are connected by fasteners forming the track panel structure. Along the track, supports for the rails by fasteners, and the restraints of the rail and transmitting characteristics are not the same in different support positions. In addition, the sections of railhead, rail web and rail foot are different along the rail and the distance is also different from wheel-rail excitation position. Therefore, there would be some differences for vibration of the rail at diverse positions.

Considering the space distribution characteristics of rail accelerations, two sections along the track are chosen, one located above sleepers and the other between the two sleepers, as shown in Figure 5a. At each rail section, 12 acceleration sampling points, located in the railhead, rail web and rail foot respectively, were chosen as shown in Figure 5b. Half of the sampling points are at each side of the rail section, six at the track side and six at the field side. Two sampling points at the rail head are located 16mm and 25mm below the top surface, and two measuring points at rail web are located at the upper part of the rail and at the neutral axis. The last two are located on the rail foot.

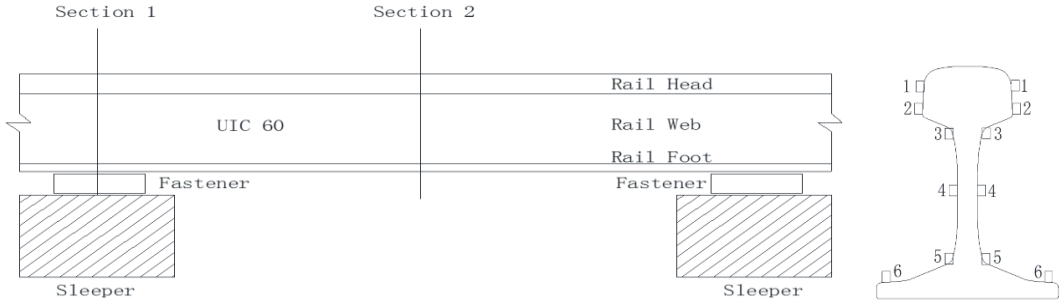

Figure 5 (a) Sampling location at two section along the rail; **(b)** Sampling points across the rail

3.3 Rail acceleration sensitivity

The rail acceleration time-history curve for the vehicle with axle load 22 tonnes and travelling speed of 160 km/h running on a ballasted track is shown in Figure 6. It is clearly seen that rail accelerations are increasing while the train dynamic load is getting close to the test section. When the load is in the test section, the rail accelerations reach a maximum value. When the load departs the test section, rail vibration accelerations attenuate constantly, and gradually return to zero. It is worth noting that, the impacts of the wheel on the railhead instantaneously transfer to rail web and rail foot. Because of the huge impact of the wheel-rail contact, the acceleration of the railhead is much bigger than rail web and rail foot and the values of the acceleration of the rail web and rail foot are much closer. Note that the subgrade base in the model is taken as fixed and hence the effect of the soil and the underlying medium in damping the high frequency vibration is not considered.

The measuring point of rail acceleration peak value above sleepers is shown in Figure 7. It is obvious that rail accelerations at the same position inside and outside are almost the same. For the test section above sleepers (Section 1), because of the constraint of fastener plates and local buckling effects of elastic bars, the peak acceleration values of rail acceleration are much closer for the two points in the rail foot. For the rail acceleration at Section 2, the acceleration at No.6 on the edge of rail foot are bigger than that of No.5 in rail foot centre point. This could be due to the cantilever position of sampling No.6 from the rail web.

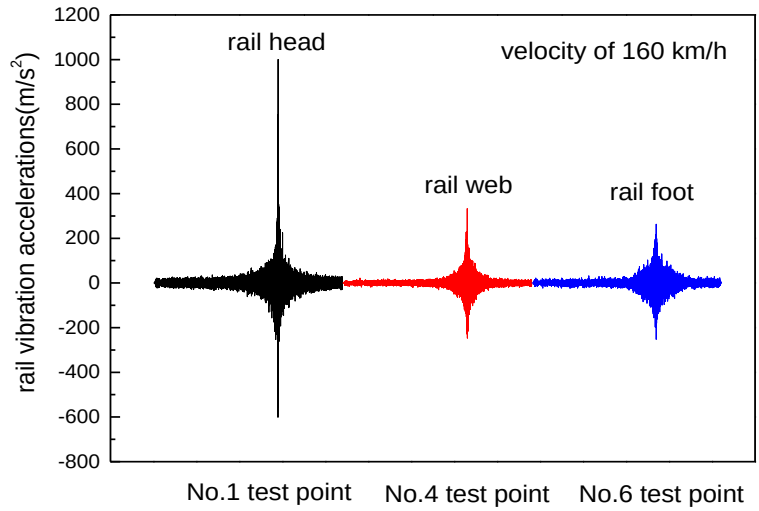

Figure 6 Rail vibration acceleration

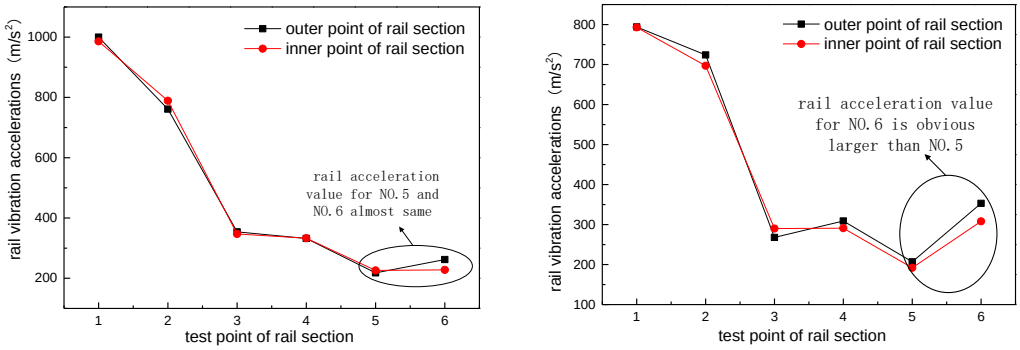

Figure 7 (a) Rail acceleration peak value at Section 1 **(b)** Rail acceleration peak value at Section 2

3.3.1 Effect of train speed

With increase in train speed, the impact from wheel to rail becomes more apparent, and the magnitude of the wheel-rail forces increases. In the multi-body dynamic software Gensys, the track is considered ideal i.e. track irregularities of any wave length and rail roughness are not considered. With an ideal track model considered, the wheel-rail forces increase slightly for various train speeds. The wheel-rail vertical forces at the speed of 100,120,160 km/h are predicted and the acceleration time history is calculated. The rail acceleration peak values and the time history curve of the rail acceleration are shown in Figures 8 and 9, respectively.

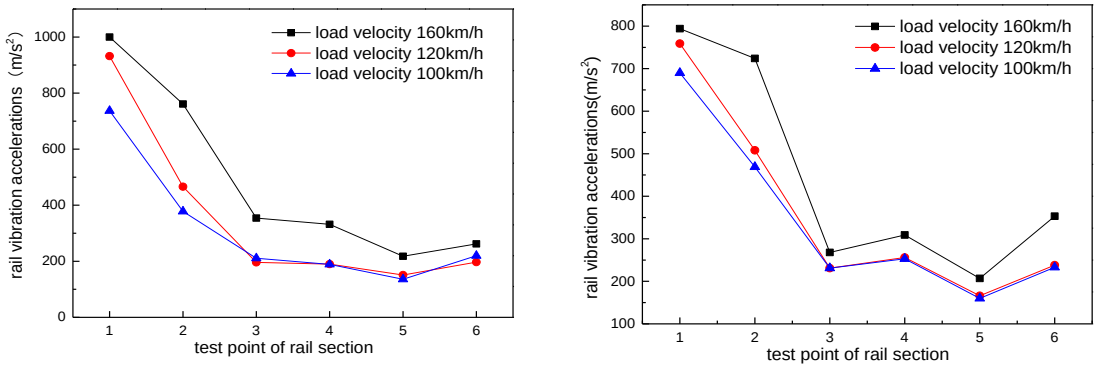

Figure 8 (a) Rail acceleration peak value above sleepers **(b)** Rail acceleration peak value between two sleepers

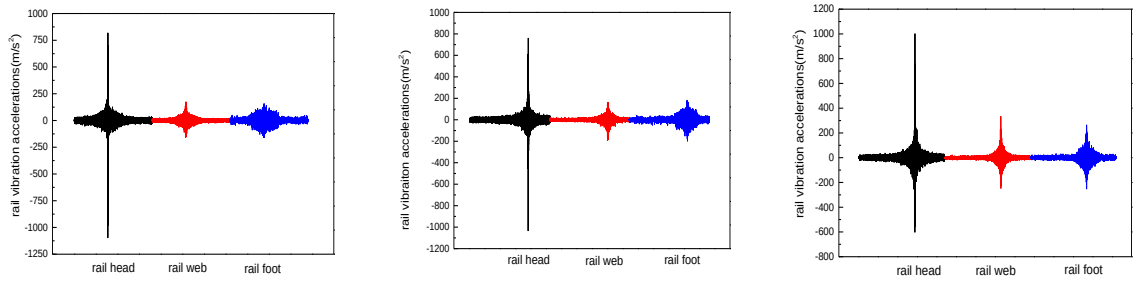

(a) Train speed 100km/h (b) Train speed 120km/h (c) Train speed 160km/h

Figure 9 Rail acceleration for various train speeds

Considering the consistence between track side (inside) and field side (outside) rail accelerations, and considering the practicality of the sensor positioning in real field, only the outside vibration accelerations were analysed. It is observed as in Figure 8 that the rail acceleration at section above the sleeper is larger than the acceleration between two sleepers for the different speeds analysed. Furthermore, increasing the train speed resulted in a larger impact on the rail section, thus the acceleration at different sampling spots of the rail will be different.

3.3.2 Effect of track irregularity

Existing researches have shown that track irregularity is the main excitation source of wheel-rail impact vibration, (Thomas K, 2009), and track vertical irregularity has bigger influence on the wheel-rail vertical force. In the multi-body dynamics model Gensys, vertical track irregularity spectrum is included as excitation source in the track model and calculation results show that wheel-rail vertical force increases significantly, whose peak increases by about 20%. Based on the calculation of the FE model using the imported wheel-rail force with track irregularities, the rail accelerations was analysed.

The peak values of the rail acceleration at sampling points Section 1 and Section 2 is shown in Figure 10. It shows that the acceleration at the railhead increases when track irregularity is considered. This is not as such evident on the other sampling points on the rail web and rail foot.

Overall, it can be seen that the wheel rail impact vibration is more apparent under track irregularity in each test section, with the peak also increasing substantially.

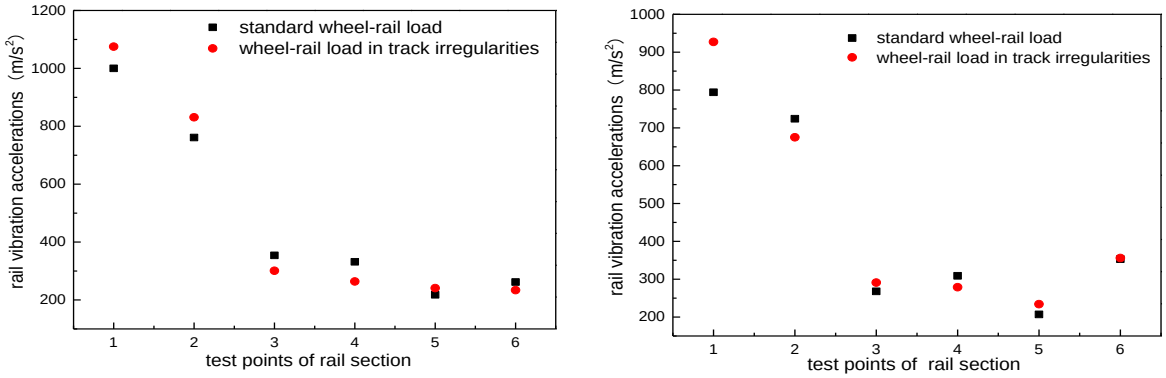

(a) Test section above sleepers (b) Test section between two sleepers

Figure 10 Rail acceleration with track irregularities

3.3.3 Effect of wheel-rail contact patch offset

Wheelset hunting is a common phenomenon that will appear in railway operation. This phenomenon could cause lateral motion of wheel-rail contact patch and hence the contact force location and orientation. In order to study the effect of wheel-rail contact patch offset from the nominal railhead centre position, the contact patch in FE model was offset by 10mm to the outside and 10 mm to the inside of the rail centre. Rail accelerations at the six sampling points were calculated while offsetting the contact patch.

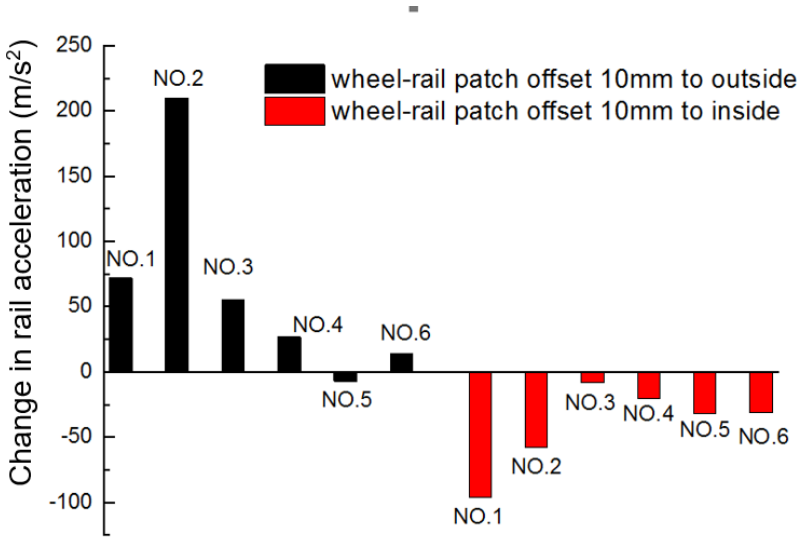

Figure 11 Change in rail acceleration from the nominal case with contact patch offset

The rail acceleration on the railhead is more sensitive to the contact patch location as shown in Figure 11. At the railhead sampling points No.1 and No.2, the acceleration shows an increase or decrease. The change in rail peak acceleration in the web and rail foot is minimum. This shows that the wheel-rail contact location influences the rail accelerations at the sampling points near the load platform while the influence decreases on other sampling points which are located on the rail web and rail foot.

3.4 Summary

This section focused on the dynamic modelling for identifying location to place the sensors and the range and frequency of the vibration as input to the monitoring system. It also covers sensitive areas and the effects of different variables on the vibration level. From the analysis, the sensitive areas of acceleration across the rail have been determined. The range and frequency of vibration accelerations are also identified. The railhead is more sensitive and an acceleration range in the order of 100-200 g is required for a monitoring system. This location is close to the wheel-rail load application and is very sensitive for train speed change, inclusion of track irregularity and location of the contact patch. The rail foot and rail web have shown more stable acceleration and the change in the acceleration value is minimal while offsetting the contact patch as well as including moderate track irregularity. This will enable to differentiate the vibration from the normal operation with vibrations due to defects on the track or the train. The acceleration range to monitor the vibration at the rail web and rail foot is much lower than the railhead and in the order of 20-40 g would be sufficient. Further, for practical field application, the location of the sensor position should not interfere with the rail regulations; hence, the rail web or rail foot are identified to be the location to mount the sensor for monitoring.

4 Instrumentation

4.1 Background

Existing methods and tools, developed more than decades ago, to monitor geometric quality of the track give some insight to a real condition of the track. This significantly helps Railway Inspectors to make qualified maintenance decisions by knowing the real state risks of the track.

This subtask is focusing on creating model infrastructure which will collect data from the sensors along the railway track and deliver these data to a dedicated server. Analysis and assessment of the data will be done in WP2. The main goals of this subtask are:

- Develop methodology for continuous monitoring of switches and crossings

- Develop system that is cheap, wireless, inbuilt, and allows real-time and continuous monitoring
- Develop and install communication, data analysis and storage system
- Test system in lab environment
- Demonstrate inbuilt technology at test sites

4.2 System architecture

The key demand of this task is to create a system, which will be fast, cheap and provide continuous monitoring on switch and crossings. Solution should be inbuilt and allow high integration into already existing infrastructure. System should provide real-time information about condition of the track to passing and monitoring trains. Big effort should be placed to deliver a maintenance-free, easy-to-install solution, which will be battery-powered and wireless. Communication system, data analysis and storage system should be part of the final solution. To ensure all of these demands, in addition to low-costs and easy integration, decision was made to use as much of already existing railway infrastructure as possible. The simplified infrastructure is shown schematically in Figure 12.

Figure 12 Concept of monitoring system

Wireless sensor containing digital accelerometer, battery and wireless module sense the vibration from passing train. Acceleration data are sent to the gateway and passed through GSM-R or WiFi to the dedicated server. The data are aggregated, analysed and stored here. Afterwards, the status information with condition state is distributed back to railway infrastructure to the operating trains through GSM-R or programmable balise. In case of identifying defect on the track, train would get this information in a real-time. The advantage of this concept is utilization of the many of already existing infrastructure which leads to lower costs and better integration.

4.3 Wireless sensor hardware platform

Wireless sensor is electronic device that will be attached on the rail track. It consists of electronic components and transmitting acceleration data to the network. Each sensor has own battery, that should power the device for many years. The important aspect of the sensor is ultra-low power consumption to achieve very long lifespan. The sensor has to be cheap, small and easy to install. The last but not least significant precaution has to be taken to the casing. The sensor will have to operate in adverse weather environment for several years and has to withstand very cold winters and very warm summers. Any damage or water ingress would lead to losing the sensor.

4.3.1 Accelerometer

Digital accelerometer will continuously monitor vibrations on the rail and once the values exceed the set level indicating the incoming train, the sensor will wake-up the rest of the electronic. Woken microcontroller switches the accelerometer to high precision measurement mode to record the samples. Once the level of acceleration drops under a specified level, the train has passed and the sensor will set back to low-power measuring mode. The rest of the electronic will finish the tasks and fall asleep. Due to this, accelerometer is spent most of the time in low-power measuring mode waiting for the incoming train. It is crucial to choose accelerometer that has very low-power consumption especially in this mode.

The big players in field of low-power and low-cost digital accelerometers are Freescale, ST Microelectronic and Analog Devices. All of these companies are manufacturing 3-axis digital accelerometers with power consumption in measuring mode up to 200 µA. The gravity magnitude is for most of the time between ±2 g and ±16 g and sampling frequency is in a range of 1 Hz to 5 kHz. After comparison of all accelerometer products with regard to requested parameters as power consumption, sensitivity, noise, range, RF transmission constraints and other features such as cost and accuracy, Analog Devices were selected as the best for the needs of this task. Although the choice of low magnitude accelerometers will not be able to sample the high acceleration peaks at the rail head, by use of such cheap accelerometers it is possible to sample useable signals to follow the signal trend and hence to detect any sudden changes in the signal trend.

The main concern was to select proper magnitude of gravity and sampling frequency. There are several working teams and many articles where the rail vibrations are sensed by very expensive instrumentation. The magnitude in some cases come up to ±500 g and sampling sometimes reach dozens of kHz. The main goal of this task is however to investigate possibility to analyse condition of the rails with limited low-cost and low-power sensors. Chraim and Puttagunta (2015) have been able to record

usable signals using a ±2 g sensor attached to the rail web capable to sample on 1.8 kHz. For this project an accelerometer Analog Devices ADXL363 was selected.

4.3.1.1 Analog devices ADXL363

Power consumption in wake-up mode with threshold selected by user and sampling six times per second consume 270 nA of energy. The regular measure mode at maximum sampling frequency 400 Hz consume 4.5 µA and about 13 µA at Ultralow Noise Mode. Data are sent via SPI in resolution 12-bit. Selectable magnitude can be set to acceleration range ±2 g, ±4 g, and ±8 g, with a resolution of 1 mg/LSB on the ±2 g range. Sensor is equipped by temperature sensor. Acceleration and temperature data can be stored in a 512-sample multimode FIFO buffer, allowing up to 13 sec of data to be stored.

During the project progress meeting it was requested to measure frequencies up to 1.5 kHz. According to Nyquist–Shannon sampling theorem, sensor must take samples at least at 3 kHz. Therefore, Analog Device ADXL313 was chosen as the final digital accelerometer.

4.3.1.2 Analog devices ADXL313

Power consumption in wake-up mode with threshold selected by user and sampling at 12.5 times per second consumes 43 µA of energy. The regular measurement mode consumes 170 µA at 3200 Hz. Data are sent via SPI in 10 to 13-bit resolution. Selectable measurement ranges can be set to acceleration magnitude ±0.5 g, ±1 g, ±2 g and ±4 g, with a resolution of 1 mg/LSB on all ranges. Acceleration data can be stored in 32-sample multimode FIFO buffer allowing up to 10 milliseconds of data to be stored.

ADXL313 in comparison with ADXL363 produce much less noise. Power consumption is however about 170 times higher in wake-up mode and about 40 times higher in regular mode. Generally, the power consumption is very low in both cases and higher consumption on ADXL313 doesn’t lead to significantly higher consumption of battery (related to 8.5Ah battery). Situation is however much worse due to amount of data that needs to be transmitted over the wireless network. ADXL313 producing eight times more data than ADXL363 which leads to rapid higher consumption. Therefore, possibilities of pre-processing of data directly on wireless sensor is investigated!

4.3.1.3 Other digital accelerometers possibilities

In the cases when the magnitude of digital accelerometer is out of the range and no usable signal is sampled, other digital accelerometer options should be evaluated:

- ADXL312 - no needed to change PCB layout, magnitudes ±1.5 g, ±3 g, ±6 g and ±12 g
- ADXL345 - PCB layout must be changed, magnitude ±2 g, ±4 g, ±8 g and ±16 g
- ADXL375 - PCB layout must be changed, magnitude ±200 g

Note - All sensors above are 3-axis digital accelerometers capable to sample at 3.2 kHz.

4.3.2 Thermometer

Each wireless sensor is fitted with temperature sensor. Information about local temperature in a measuring point can extend the acceleration data for a better post-processing and analysis. Type of sensor was selected by IQRF practices (IQRF TR-76D. IQRF), this sensor is equipped in many IQRF RF modules except the one is used and it has a direct support by IQRF operation system.

Microchip MCP9808 is digital temperature sensor which converts temperatures between -40°C and +125°C to a digital word sent by I2C with maximum accuracy ±1°C (typ. ±0.25°C). Maximum accuracy at the range -20°C to 100°C is ±0.5°C (typ. ±0.25°C). Typical operating current is 200 µA and typical shutdown current is about 100 nA.

4.3.3 Data acquisition

Digital accelerometer ADXL313 produce 3200 samples per second on each of three axes where each sample has about 13-bits in full resolution mode. If the amount of data cannot be reduced, 192 kilobytes will be collected in 10 seconds. These data needs to be stored before they will be transmitted or pre-processed. Hence large and fast memory is requested. SRAM memory was selected against EEPROM due to unlimited writing/reading cycles, zero waiting time and power efficiency. Due to many benefits, the Microchip SRAM memories were selected to be used at the device. Producer offers different memory capacities with the same pin out for a reasonable price.

Microchip 23LC512 is serial SRAM memory with capacity 512kbit and SPI interface up to 20 MHz. Operating current is typically 1 mA (max. 10 mA) and standby current is about 1 µA (max. 4 µA). Data are organized in 64k x 8-bit cells and are accessible

through bytes, pages and in sequential mode. Memory has zero write time and support unlimited reads and writes to the memory array. Operational temperature is from -40°C to +85°C.

4.3.4 Battery

To power up the wireless sensors for several years, special battery cell had to be used. Most of the classic batteries would self-discharge in a few years even if they are not used. Therefore, the primary lithium-thionyl chloride batteries invented by Adam Heller were picked. These batteries are well suited to extremely low-current long-term applications where long life is a must.

The default cell choice for the system is EVE ER26500T, which is industrial Lithium-thionyl chloride (Li-SOCl2) cell of size C having a large energy density with very low self-discharge characteristic. Battery is providing stable voltage around 3.6 volts for whole life of the cell. Voltage is dropping to 2.7 volts at the low temperatures around -30°C. Energy capacity of the battery is 8.5 Ah with the price about 10 dollars.

Alternatively, an EVE ER34615T with 19 Ah of energy can be used. This battery is bigger than previous one, the size is D. Price also rise up to a 15 dollars for a cell. This battery is less prone to low temperatures and the voltage is falling to about 3 volts at -30°C.

4.3.5 Power Source

The wireless sensor will be battery powered. Output voltage necessary for proper function of all the components needs to be in range 3V - 3.3V[1]. Especially in cold winters the voltage of power cell can drop down under 3V. Therefore, the Buck-Boost DC/DC convertor LTC3335 was chosen to deliver stable voltage on an output.

Microchip LTC3335 is a Nano power Buck-Boost DC/DC convertor which is especially designed for long-term battery powered applications. Source is delivering stable output voltage that is either greater or less than the input voltage magnitude. Therefore, sensor will work either in very cold weather when the voltage of battery cells drops down below the selected three volts. The regulator has very low Input Quiescent Current 680nA at Output in Regulation at No Load. Output Voltages are selectable to 1.8V, 2.5V, 2.8V, 3V, 3.3V, 3.6V, 4.5V and 5V. Good feature is Programmable Peak Input Current of 5mA, 10mA, 15mA, 25mA, 50mA, 100mA, 150mA and 250mA. Due

[1] Due to change in datasheet IQRF TR-76D, device can be powered already from 2V (2.7V with TMP sensor)

to these settings it is possible to discharge battery in a very controlled way to prolong the life span of the battery. Efficiency of the power source is up to 90% which is reached at extremely low currents. Integrated Coulomb Counter is great feature for continuous and precise monitoring of how much energy is already consumed.

The Linear Technology LTC3335 like the other power sources requires passive components for proper function. These components are setting the parameters of the source and determine its properties. A schematic of LTC3335 is shown in Figure 13.

Selected values by HW design

U_{IN} = BAT = 3.6 V
U_{IN_MIN} = BAT_{MIN} = 2.7 V (-30°C)
U_{OUT} = 3 V
I_{PEAK} = 100 mA (I_{PEAK} recommended by battery datasheet)
L_{REC} = 100 µH (L_{REC} recommended for I_{PEAK} = 100 mA)
t_{fs} = 11.47 µs (t_{AC} must not exceed the max full-scale time)

Inductor selection

$$L_{MAX} = 0.8 \cdot \frac{BAT_{MIN} \cdot L_{REC}}{1.8} = 0.8 \cdot \frac{2.7 \cdot 100\mu}{1.8} = 120\ \mu H$$

The maximum allowed value for inductor is 120µH, but typical manufacture tolerance for these inductors ±20% has to be taken in count. With consideration, that these values are counted with minimum battery voltage 2.7 volts at -30°C and ILOAD = 20 mA, it is possible to use some reserve for even lower temperatures. Therefore, selecting recommended value **L_{REC} = 100 µH**.

Switching times of power FETs (H-Bridge)

$$t_{AC} = AC(ON) = \frac{I_{PEAK} \cdot L}{BAT} = \frac{100m \cdot 100\mu}{3.6} = 2.\overline{77}\ \mu s \qquad t_{AC} \cdot 1.2 < t_{fs}$$

$$t_{BD} = BD(ON) = \frac{I_{PEAK} \cdot L}{V_{OUT}} = \frac{100m \cdot 100\mu}{3} = 3.\overline{33}\ \mu s$$

Load current capability[2]

$$I_{LOAD(MAX)} = \frac{I_{PEAK}}{2} \cdot \frac{BAT}{BAT + V_{OUT}} = \frac{100m}{2} \cdot \frac{3.6}{3.6+3} = 27.\overline{27} mA$$

Coulomb counter errors

$$q_{AC(ON)} = \frac{I_{PEAK} \cdot t_{AC}}{2} = \frac{100m \cdot 2.77\mu}{2} = 138.5\ n\text{A}$$

Selection of input and output capacitor

[2] Actual deliverable current is lower due to finite RDS(ON) of power FETs A, B, C, and D, as well as inductor DCR

Recommended ceramic capacitor **C_{IN} = 10 µF** and **C_{OUT} = 47 µF** was selected. However, in future revisions, the output capacitor may be replaced by higher value low leakage aluminium electrolytic capacitor or by super capacitor.

$$t_{SLEEP} = C_{OUT} \cdot \frac{V_{DC\_HYS}}{I_{LOAD}} = 47\mu \cdot \frac{10m}{20m} = 23.5\ \mu s$$

20 mA => 23.5µs; 43 µA => 10.9ms

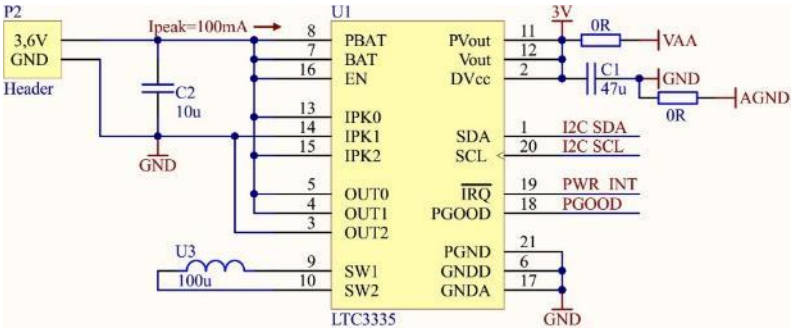

Figure 13 Schematic of LTC3335

4.3.6 Wireless (RF) module

The wireless communication is connection between two or more subjects realized without help of wires, cables or any other forms of electrical conductors. The carrier medium can be optical (light), radio (radio frequencies) or ultrasonic (sound). The communication distance can be between few meters and thousands of kilometres.

For a given task, it is expected that, in the worst-case scenario, there will be 192kB of data from each sensor for every train pass. This situation occurs when all 3-axes sample at 3,2 kHz for about 10 seconds. All these data needs to be transmitted over hundred meters from the sensors placed on a track to the gateway. The chosen solution has to be reliable, low-cost, and power-efficient to sustain many years operation on battery. With regard to these requirements, the most suitable solution is to use some of the embedded low-power RF modules that perform well in given environment and can be relatively cheap, small and reliable. There are many products implementing various protocols as WiFi, ZigBee, BLE, UWB, LoRa, IQRF and others. With so many standards and different protocols it is not easy to find the proper balanced solution especially for battery powered application. Comparing the pros and cons of each solution, the IQRF platform, see Figure 14 was chosen as the most appropriate.

The IQRF TR-76D is affordable RF module with costs around 8,5 dollars in 1k+ quantity, that can be simply integrated into other PCB design by SMT mounting. The module communicates at 868MHz with GFSK modulation and data rates up to 19,836 kbps. Other data rates (up to 500kbps) will be implemented in some of the following updates. The very low power consumption (TX 8.3-19 mA/ STD RX 12,3mA/ LP RX 233µA /XLP RX 15µA), great RF IC sensitivity -106dBm, RF output power 12,5 mW,

communication range 500m[3]/1100m[4], and a tiny module size 15.2 x 14.9 x 3.3 mm makes this module a great option. Module is fully controlled by user application program where developers may use inbuilt operation system to speed up the design. IQRF ecosystem offers also easy integration with other IQRF devices such as gateways, cloud and others as described in Section 4.5.

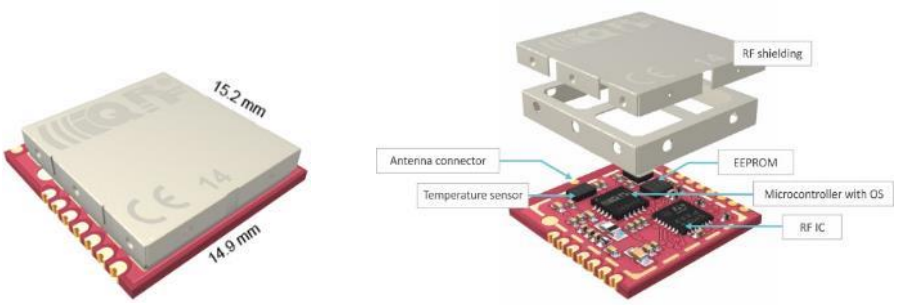

Figure 14 IQRF TR-76D [*from IQRF TR-76D. IQRF (cited 2016)*]

RF communication is performed in SRD-860 band on stated frequencies:

- RF Channel 1 52 (868.35 MHz with 20 kHz spacing)
- RF Channel 2 63 (869.45 MHz with 20 kHz spacing)

4.3.7 Printed Circuit Board (PCB)

The schematic circuit layout shown in Figure 15 and in the Appendix is manufactured in two batches, the first ten boards as a prototype and second batch in bulk quantity for full scale tests. It is expected that the cost for producing such boards in great quantity (>1000 boards) would be 0.2 to 0.5 Euros per piece.

[3] 2x TR-76DA plugged in DK-EVAL-04x 1,6m vertically above ground with reflective planes at >100m distance

[4] same as in [3], just TR-76D plugged in DK-EVAL-04x through RNG-EXT-01 adapters (IQRF products)

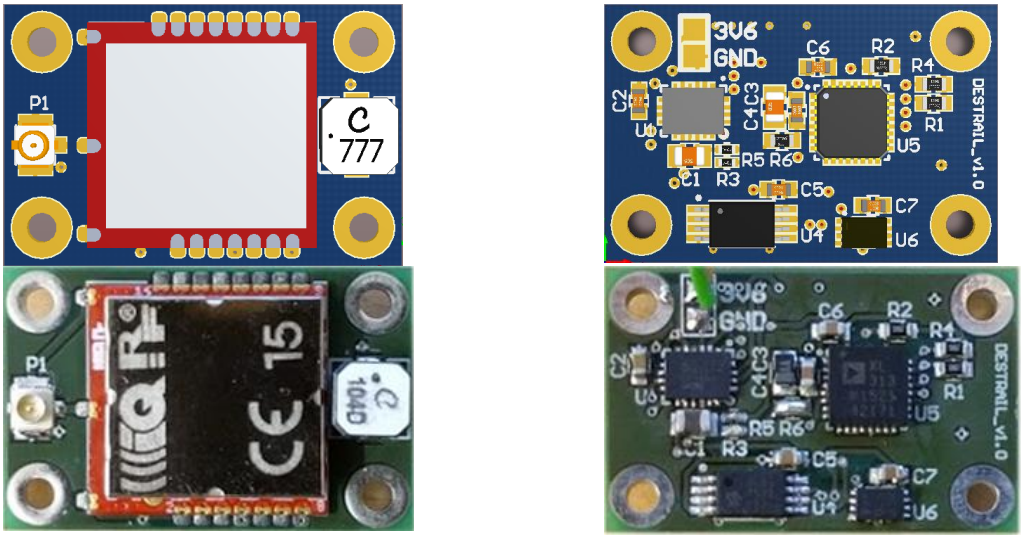

Figure 15 Printed Circuit Board (PCB) simulation (top), manufactured board (bottom)

4.3.8 Casing

Design of wireless sensor casing is one of the most crucial and easily most underestimated part in many cases. Designers in similar projects often tend to focus on electronic (HW/SW) part despite the fact that one dysfunctional element in the chain will cause the entire system not working at all. However, faulty design of the wireless sensor casing can cause serious issues and can significantly affect performance of the system, such as:

- Excessive mechanical stress (e.g. close to antenna) that will cause
  - water/moisture ingress into the box which would damage electronic/battery
  - box disintegration
  - filtration of/additional vibrations
- Higher costs, worst mounting properties, dropout of the box from the rails
- RF signal damping
  - un-appropriate polarization
  - location close to conductive planes/ground
  - radiating energy into the wrong directions
- Damage by train, during grinding or other maintenance tasks

Therefore, the design of construction and choice of material has been done with care.

The recommendation of the numerical modelling work (ref. Section 3) on the location of the wireless sensor on the rail is also considered (Cai and Kassa, 2016). Further the rail IMs regulation with regard to free clearance was considered based on the discussion with the Danish and Norwegian Rail Administration.

The goal of the project is to provide wireless sensors which will be cheap and easy to install. Therefore, it was decided to place acceleration sensor, battery and antenna into one single casing to achieve compact design. Antenna was placed as far from conductive and ground plane as possible and into horizontal position as shown in Figure 16. This should help to have signal less affected by conductive materials that are all around and should help with signal propagation to all direction around the transmitting position.

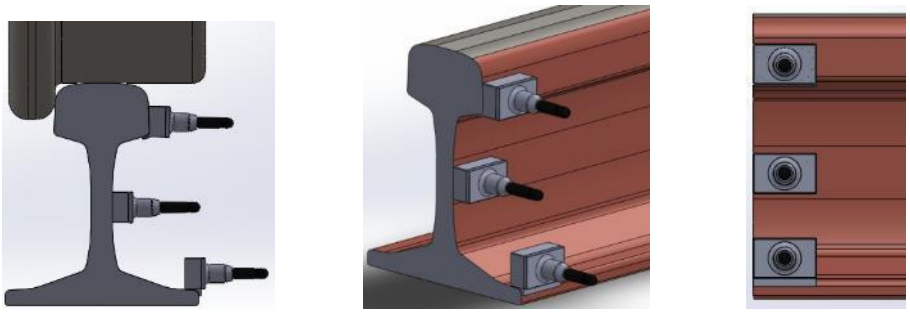

Figure 16 Illustration of possible sensor placement; horizontal antenna, sensor, and battery all in one compact casing

There was concerns from railway infrastructure managers about the railhead position and the size of the sensor. Placing anything on railhead is generally considered as a bad practice. Therefore, it was decided to create as small casing as possible and place it on the rail web, rail foot and the sleeper. The battery was placed separately in a battery casing that will be buried into the ballast and connected to the sensor by cable. With this solution, authorization is granted by Banedanmark (railway administration in Denmark) to install the sensors on Tommerup test-site station in Denmark.

4.4 Power consumption of wireless sensor

Wireless sensor has to have a very long operational lifetime to be cost-effective. Thanks to modern microcontrollers, power efficient RF modules and battery-types like Li-SOCl2 primary cells, the various application may be powered for 10 or more years. All that depends on the average power consumption, working environment and parameters of the battery cell.

Despite the fact that the power consumption of each electronic component used in wireless sensors design is known and the working conditions together with average self-discharge rate of the battery can be estimated, the real power-consumption will always vary on many of parameters. The amount of data that needs to be transmitted,

changes of temperature and the level of optimization are some of the significant factors for such wide variation. As a brief guidance for the expected consumption, Table 2 shows the calculated expected data. However, the real revealing data will be obtained from a long-term monitoring (Coulomb counter of LTC3335).

The case of study		**Results**	
Trains per day	10	Battery capacity	7700 mAh
Data per train	192 kBytes	Consumption per year	1 746 mAh
RF datarate	2,5 kBs	**Lifetime**	**4,41 years**

			Sleep	Process	RX LP	TX STD	
IQRF TR-76D	time	[min]	1 404	1	21	14	**Total**
	current	[µA]	1	1 600	233	19 000	
	per day	[µAh]	23	27	83	4 496	4 628 µAh
	per year	[mAh]	9	10	30	1 641	1 689 mAh

			Sleep	Wait	Meassure		
ADXL313	time	[min]	1 338	100	1,667		**Total**
	current	[µA]	0,1	43	170		
	per day	[µAh]	2	72	5		79 µAh
	per year	[mAh]	1	26	2		29 mAh

			Sleep	Operating			
23LC512	time	[min]	1 440	0,016			**Total**
	current	[µA]	2	2 000			
	per day	[µAh]	48	1			49 µAh
	per year	[mAh]	18	0			18 mAh

			Sleep	Operating			
MCP9808	time	[min]	1 440	0,005			**Total**
	current	[µA]	0,1	200			
	per day	[µAh]	2	0			2 µAh
	per year	[mAh]	1	0			1 mAh

			Sleep	Operating			
LTC3335	time	[min]	1 438	2			**Total**
	current	[µA]	0,68	360			
	per day	[µAh]	16	10			26 µAh
	per year	[mAh]	6	3			9 mAh

Table 2 Power consumption of wireless sensor

4.5 Transmission and communication network

A transmission network is a collection of terminal nodes and transmission links between them allowing the process of data propagation through the transmission medium. Each terminal in the network has unique address which helps to forward data to the correct recipients.

The RF modules selected in Section 4.3.64.3.6 offers simple integration with others IQRF components. Developers may pick and program one of the IQRF gateway which automatically forward all of the passing data right into the IQRF Cloud. From there, all information may be collected by Cloud API and stored on server, see Figure 17 for

graphic illustration. The possibility to utilize already built structure will rapidly speed up development and will allow to deliver requested solution in a very limited time.

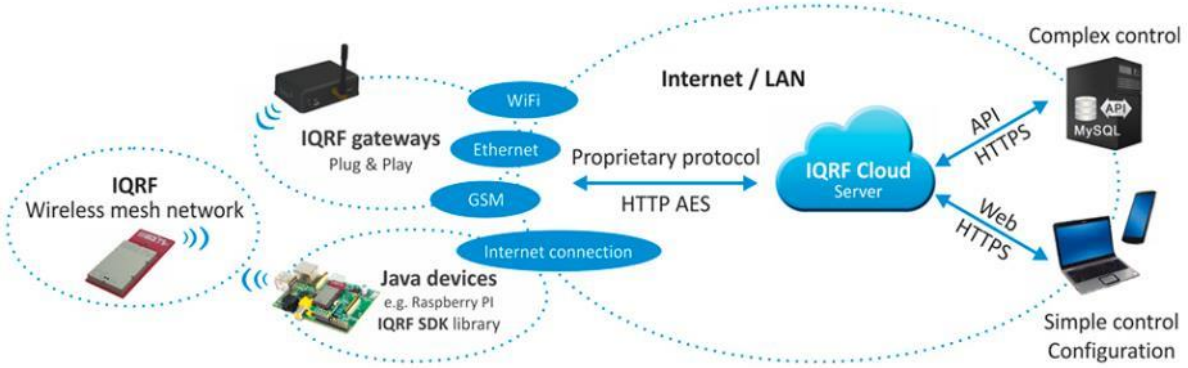

Figure 17 IQRF network [*from IQRF Cloud (cited 2016)*]

4.5.1 Gateway and Cloud

Gateway is the main element which has full control over all communication in the sensor network. This type of communication model is called master-slave or coordinator-node. Wireless sensors can't perform any actions without coordinator's commands. Gateway is responsible for wireless sensors actions, data consistency and for forwarding of such data and other information to the internet storage (cloud or webserver).

Due to the complexity of the system with respect to a given time, a 3rd-party gateway was originally used for this task. One of the three IQRF gateways based on WiFi, GSM (GPRS) or Ethernet can be used. Gateways are programmed by user application and they automatically forward all incoming data to the IQRF Cloud. Communication is secured by AES encryption as shown in Figure 17. Once the data reach the IQRF Cloud, they can be accessed directly by HTTPS connection from any device connected to the internet or by IQRF Cloud API.

Because the Ethernet and WiFi gateways are not released yet, GSM gateway was used for development of the system. This gateway will not be deployed due to limited data throughput that the GPRS has, but it is used for implementing of IQRF Cloud API to the web server.

It is expected that future gateway will operate within GSM-R and will utilize already existing railway network. However, at the moment, it would be too ambitious to build a gateway that communicate over GSM-R. Therefore, a universal gateway, that will be highly scalable and will allow easy and powerful integration into already created structure becomes the goal. Such gateway will send data directly into the Web based Content Management System (WCMS) database without use of cloud layer as

originally planned. The resulting communication will be simplified and it will further reduce the system delays. The gateway was built of these components:

- Computer (coordination and processing) Intel® Compute Stick STK1AW32SC
- Communication: Wireless sensors <=> Gateway IQRF GW-USB-06 (PCB antenna)
- Communication: Gateway <=> WCMS ZTE 4G MF831

This gateway was tested with rest of the system, at Tommerup test-site in Denmark. The system that worked while tested in a laboratory environment didn't perform well in the field test. The gateway was modified with more reliable and powerful components based on experience from Tommerup test-site. External antennas were added and the gateway was enclosed into its own cabinet. This way the gateway is more universal since it doesn't rely on other cabinets that have to be on place and can be located always at the best spot with regards to the RF system as illustrated in Figure 18.

The modified gateway version is built of:

- Casing
  - pole, cabinet, cabinet heater, thermostat
- Electronic
  - Intel® Compute Stick STK1AW32SC
  - IQRF CK-USB-04A + Wireless sensor (combination is similar to IQRF GW-USB-06). External antenna and temperature sensor can be use
  - Huawei 4G E392 (instead of ZTE 4G MF831)
- Antenna
  - IQRF AN-08 outdoor, directional, SRD-868, 10dBi, Yagi
  - Sonstige ART5949 outdoor, omnidirectional, 4G, 12dBi

4.5.2 Web Content Management System (WCMS)

The Web based Content Management System will be the last main part of the communication chain. All data from the wireless sensors will be stored, analysed and delegated from this place. Only authorized users will have simple access through the https protocol anywhere from the Internet.

The necessity of the WCMS is due to the fact that IQRF Cloud store data as data packets (n x 64 bytes) and the capacity is limited to last few thousands of the records. Working with these data would be unpractical, complicated and data would be erased at a certain moment.

WCMS will implement the IQRF Cloud API and will periodically collect these data from the cloud. Data will be stored in a compact format with all related details which will give the ability to display information in a context. The WCMS will be based on Drupal 7, see Figure 19, and will implement interface for direct access to the database. It also speeds up subsequent work with data from the external software such as MATLAB.

All communication is secured by https protocol and self-signed certificate (RSA 2048-bit public key), that is provided in advance to the granted users. Granted users connected to internet may access to this website by any type of device capable to display web-based content. The server IP address (217.16.187.219) is assigned to the domain name https://monitoring.destinationrail.eu.

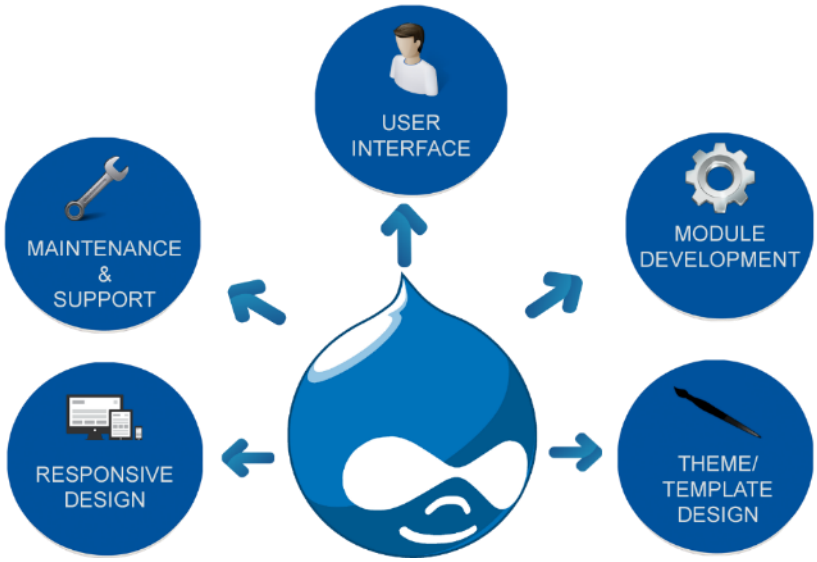

Figure 19 Drupal 7 [*from www.worldranksolutions.com (cited 2016)*]

Webserver currently implements the base functionality as:

- Registration and secured access (https) for granted users (Figure 20)
- Gateway location history
- AJAX calls for loading the dynamic content (JS, JSON)
- Data page with all collected acceleration data viewed in graph (Figure 21)
- Direct access to the database from 3rd party software's such as MATLAB

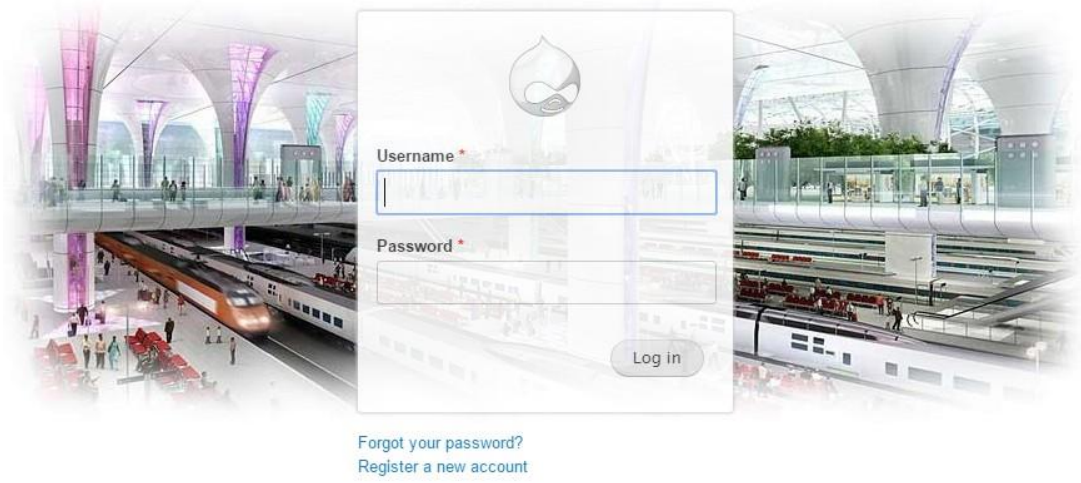

Figure 20 Login page of WCMS

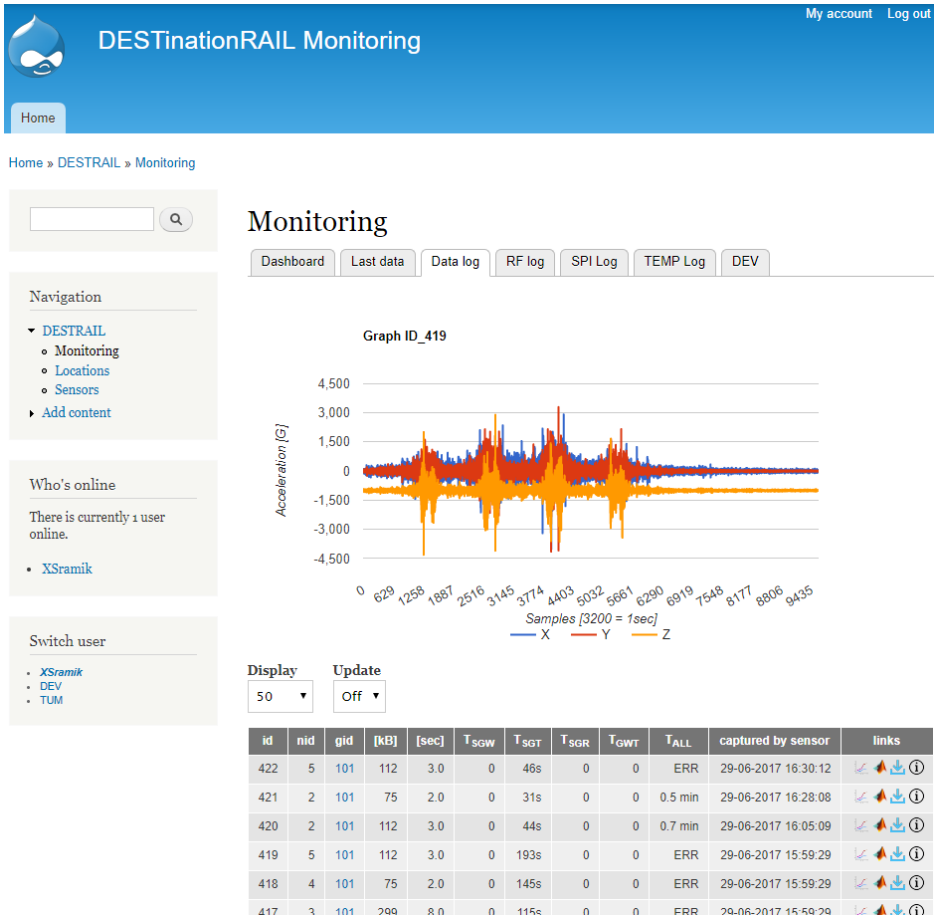

Figure 21 Website features

5 System evaluation and validation

This section discusses the concept feasibility test and the whole system assessment from field test. The problems that arise during the development of each parts of the system and suggested modifications are also presented.

5.1 Test of concept feasibility

The preliminary test of concept feasibility was performed during the first stage of the task. This was realized to evaluate the crucial components and their parameters. The main concerns were about the electronics capability to sense the incoming train, accelerometer response on an overpassing train and ability to transmit acquired data over the radio frequencies. Before the system was deployed at Tommerup test site in Denmark, it was fully tested for several days in a lab and outdoor environment.

The measurement chain was assembled by different evaluation boards as shown in Figure 22. The Wireless Sensor part consisted of chosen accelerometer EVAL-ADXL313-Z-ND, evaluation board DK-EVAL-04A equipped by battery, and RF module TR-72DAT connected into this board. Data were transferred wirelessly to the second RF module that was connected into the programmer CK-USB-04A and future on by USB cable to the computer.

Figure 22 Schematic of the measurement chain

As the first trial, the accelerometer's sampling frequency was set to 400Hz while the magnitude of acceleration was set to ±2g (1024 values/LSB). The EVAL-ADXL313-Z-ND was equipped by four magnets with a thrust force 7kg each and placed on the rail web with total aggregated force 28kg, as shown in Figure 23.

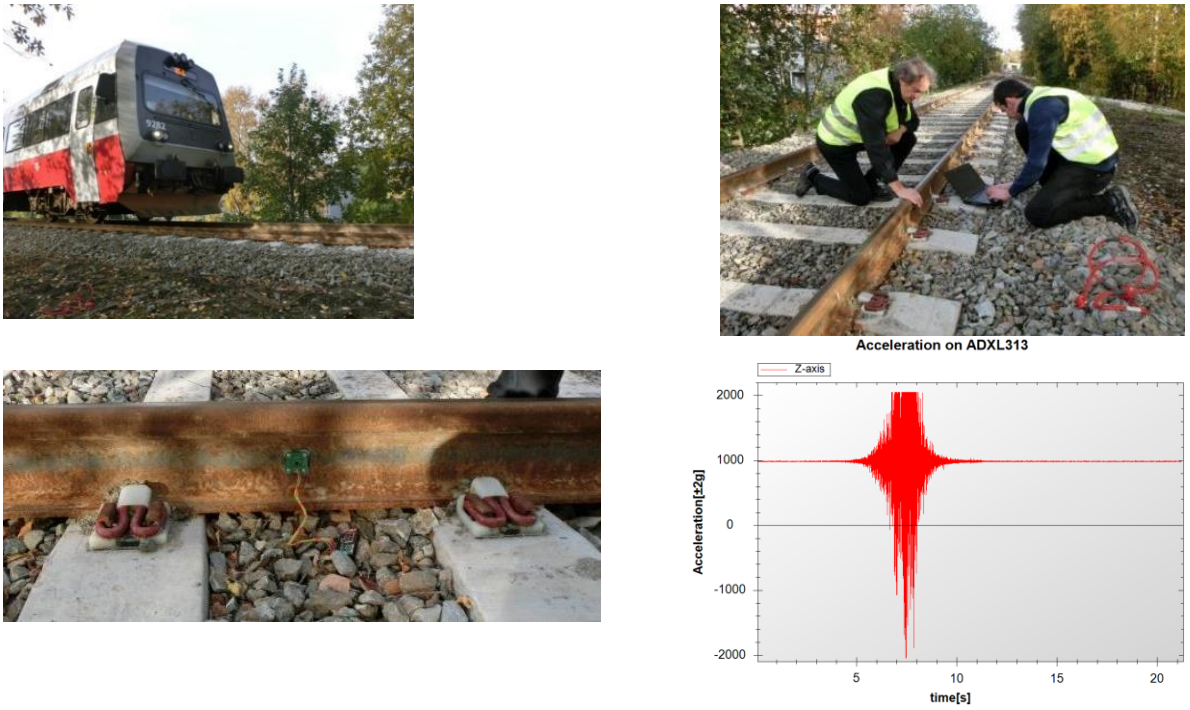

Figure 23 Passenger train passing over the test point (top left), work on the rails (top right), ADXL313 Evaluation Board attached on rail web (bottom left), acceleration sampled (bottom right)

Measuring was triggered automatically by incoming train once the level of acceleration crossed over the specified threshold level. Data were automatically transmitted over the whole structure into the C Sharp application running on a computer. The application recorded these data into the RAW file and displayed them in a chart.

Two passenger train passings in both directions were measured on a spot close to the railway station. The speed of the train over the sensor in both directions was about 10 kmh-1. Incoming train was slowing down to the station and passed over the sensor, see Figure 24. Then the train stopped at the station. It becomes visible that the magnitude of acceleration at scale ±2g has overrun and the range should be increased. The acceleration magnitude was set to ±4g with no additional cost.

5.2 Antenna test

To be able to use the gateway outside of controlled environment e.g. faraday cage, all parts involved in signal propagation had to be measured in an antenna lab. This allowed to properly set the output constants and verify that not more than 500mW ERP will be radiated from the antenna. This is regulated by legislation to prevent RF interference between various systems, that might be dangerous especially on the railway.

Antenna lab contained reference antenna with known gain (see Figure 24, red antenna) and known distance from tested antenna. This was enclosed in the room with relevant parameters for RF systems tests. Due to known RF attenuation in used coax cables and air of known distance, the correct parameters were calculated and set to the gateway to reach the goal ERP. Gateway were than verified against the legislation.

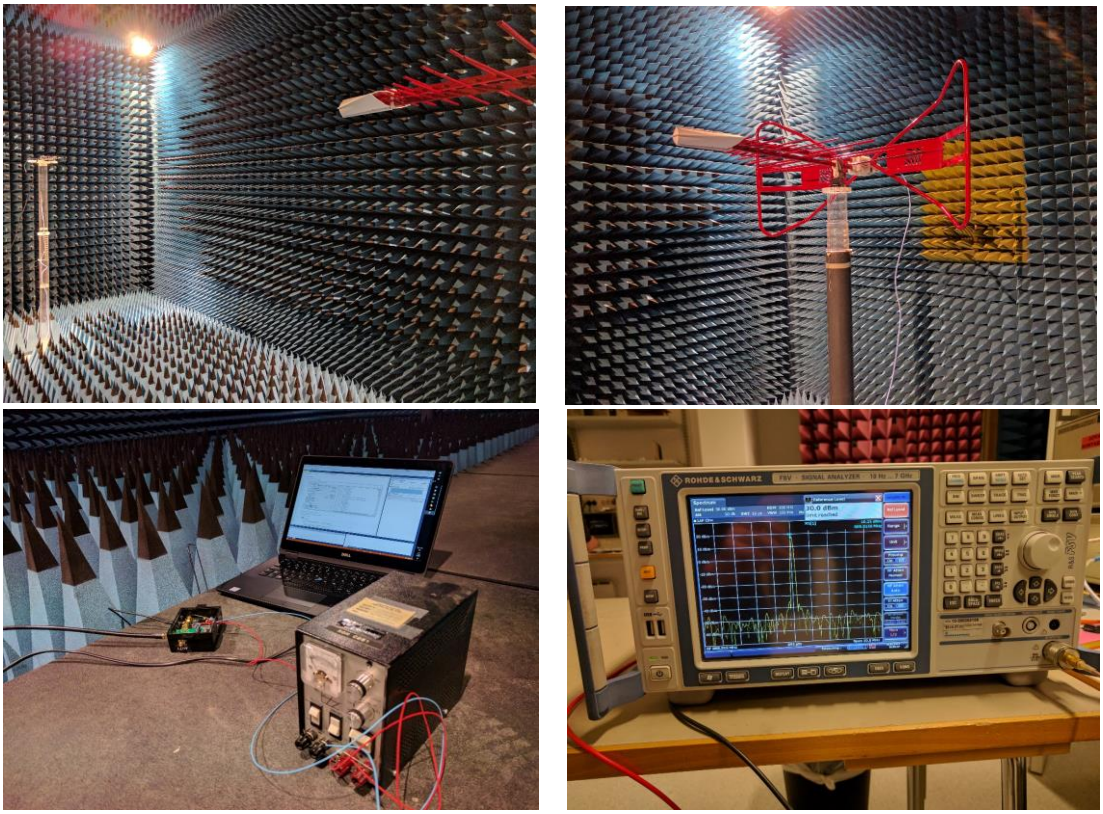

Figure 24 Antenna laboratory test

5.3 Rail coverage test

Rail coverage test was held on a track at Norwegian national railway infrastructure (Bane NOR). Sensors were deployed in 30, 60 and 90 meters distance from the gateway that was attached on a pole of height 1.3 and 2.2 meters, see Figure 25.

The main purpose of this test was to test the reliability of the communication between sensors and gateway. The sensor casing, both the old and new sensor casing were tested. Results revealed that about 6dB difference against old web casing, which practically doubles the usable distance. Therefore, sensors in a new casing can be deployed in twice the distance while achieving the same transmission properties.

The test was conducted at a sunny day, -12°C and with snow coverage. The sensors were covered by 10cm layer column of snow, which is common during the winter at this location, didn't tend to signal dumping. Further, passing trains during the active transmission didn't seem to interfere with the active communication. Reliable

communication was achieved during the whole test with signal strength above -62dBm (with gateway on 2.2m pole).

Figure 25 Antenna coverage field-test with sensors covered by snow

5.4 Field tests

5.4.1 Tommerup test-site - Denmark

Installation of Wireless Sensors was performed during full traffic on a switch at a place called Tommerup in Denmark. Once the sensors were on place, their threshold level for incoming train was set over-the-air from nearby gateway. Afterwards, gateway was mounted in a cabinet which was already existing onsite. However, the connection between wireless sensors and gateway were not possible to establish. It was found out that the location of the gateway, which is mounted in a cabinet nearby, was not suitable for the data communication.

The most probable causes for the disruption of the communication are mutual position between sensors and gateway, several electronic system nearby used by another test campaign, conductive materials, reflective planes and other RF system antennas close by. A significant issue here has also been effective radiated power, which is just 12,5mW of energy (ERP) in 360° of horizontal plane. To address the communication problem, an own cabinet was built and mounted on a pole and outdoor antennas were placed. With that, the gateway can be placed in a proper position at the same time it addresses the needs as radiated pattern, directivity and polarization. Using a 10dBi Yagi antenna that can transmit 76.2mW of energy (ERP) in narrow beam 36° with elevation 32°, it was possible to increase the signal in radiated zone more than 68-times (Figure 26).

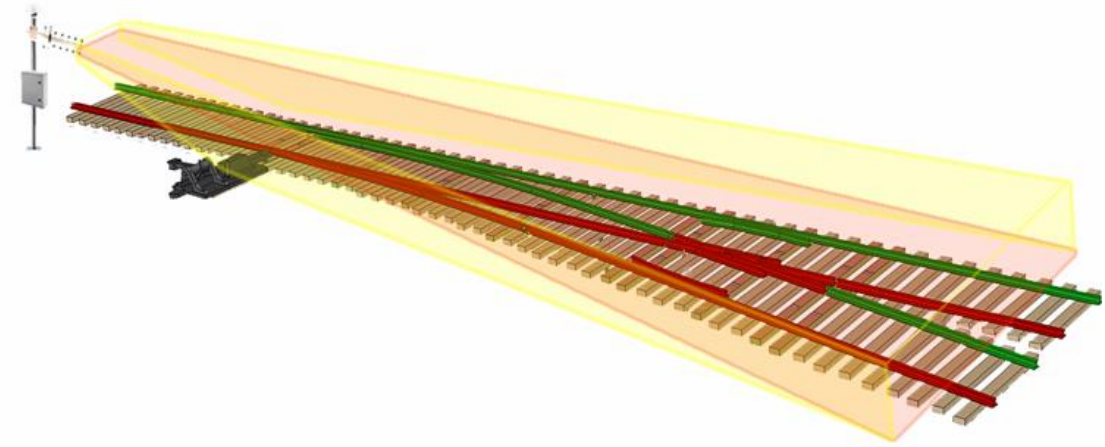

Figure 26 Gateway and external antenna – signal coverage

The field demonstration at the Tommerup station revealed some drawbacks in the system which have been corrected and deployed at the demonstration in Munich. Some of the improvements are:

- **Sensor casing** has been improved considering:
  - used material due to chemical stability over the time
  - durability against vandalism and stiffness regarding vibration dumping
  - waterproofness of the sensors
  - location of the antenna regarding the sensor on the rail
- **Gateway** has been improved to:
  - increase RF power
  - avoid signal disruption caused by a nearby objects (e.g. placing the equipment into unknown cabinets or close to the steel constructions).
  - ensure optimal signal propagation by placing the gateway to a suitable location

5.4.1.1 Sensor casing

The new sensor casing was designed to address higher requirements for chemical stability, durability, stiffness, waterproofness and signal propagation. Casing were manufactured for two sampling locations on the track – rail web and sleeper (Figure 27). Two types of rail profiles are currently supported – 54E3 and UIC60.

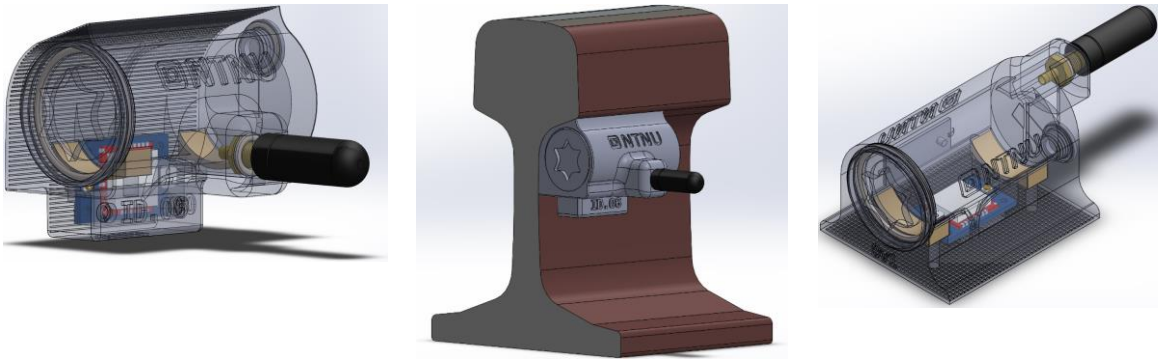

a) b) c)

Figure 27 New sensor casing on rail web (a), placement on a UIC60 rail web (b), on sleeper (c)

First measurements on a track with different environmental conditions showed improvement in signal propagation about 6dB for railway web casing. That practically double the useable distance that can be covered by signal.

5.4.1.2 Gateway

5.4.1.2.1 Placement

RF signal propagation is very sensitive to the surrounding environment and especially to objects that are in direct proximity. Therefore, to reduce the possibility of signal disruption due to nearby objects the gateway was placed in own stationary cabinet so that the near proximity environment stays the same regardless of the location.

5.4.1.2.2 Antenna

Another measure was taken by replacing the omnidirectional antenna by directional one. Yagi antenna suppress incoming signals from other directions than the main and at the same time it gains useable signal from this direction, see Figure 26. Another benefit lies in the possibility to attach the gateway with antenna directly on a catenary mast and it was found out that the amount of reflections was low.

5.4.1.2.3 Electronics

The other important step was to increase the effective radiated power from 12,5mW to 500mW that enhance the coverage of the area and improve the reliability of the RF communication. This was done by front-end module which increase input sensitivity and at the same time it gains the output signal. The whole gateway including all parts as Yagi antenna, FEM module, and RF module were taken to antenna laboratory. This was crucial to set the correct effective radiated power to the maximum allowed value

and not to violate the legislation. Test was finished by verification of the ERP parameters, refer Section 5.2.

5.4.2 Munich test-site - Germany

On 19 June 2017 a measurement campaign was carried out on one of the main railway lines around the Munich region. Frequency of trains at rush hours was around four to five trains in an hour for a single direction. The selected test site is a plain line track. Sensors were mounted at two locations to measure the acceleration parameters at the railway web and sleeper.

Each of the test positions was equipped by sensor developed within this project, with the old and new casing, and by a reference sensor which is known to give reliable data (see Figure 28).

Figure 28 System test in Munich – sensors mounted on rail and sleeper

Gateway was attached on a catenary mast at about 2.5 meters above the rail head and in about 80-meters distance from the sensors, see Figure 29. The usual average spacing between catenary masts at this location is about 70-meters. Along the rails between gateway and sensor, there was a very good coverage by signal that was above -60dBm at 80-meter distance from the gateway.

Figure 29 System test in Munich – gateway

5.4.2.1 Sensor system validation

During the one-day measurement test on the track close to Munich, data were collected from all the sensors. About 14 train passages were recorded. Sensors were positioned at rail web (P1, P2), whilst two sensors were positioned at the sleeper (P3, P4). Sensors P1 and P3 were enclosed in the new casing (white coloured casing), P2 and P4 in the old one (black coloured casing), see Figure 28. Reference sensors from the project partner TUM were positioned at the rail web (inside the rail) and on the sleeper. The data from TUM reference sensors is used for a comparison and validation of the sensors developed in this project. For data processing purpose, data from passing trains 4, 7 and 15 (time order) is processed and shown in this report. Records from other trains show comparable results.

The sensor from TUM collected data from nine train passages. These sensors are measuring single axis and were sampling on 25.6 kHz. Data records from the train 4, are shown in Figure 30.

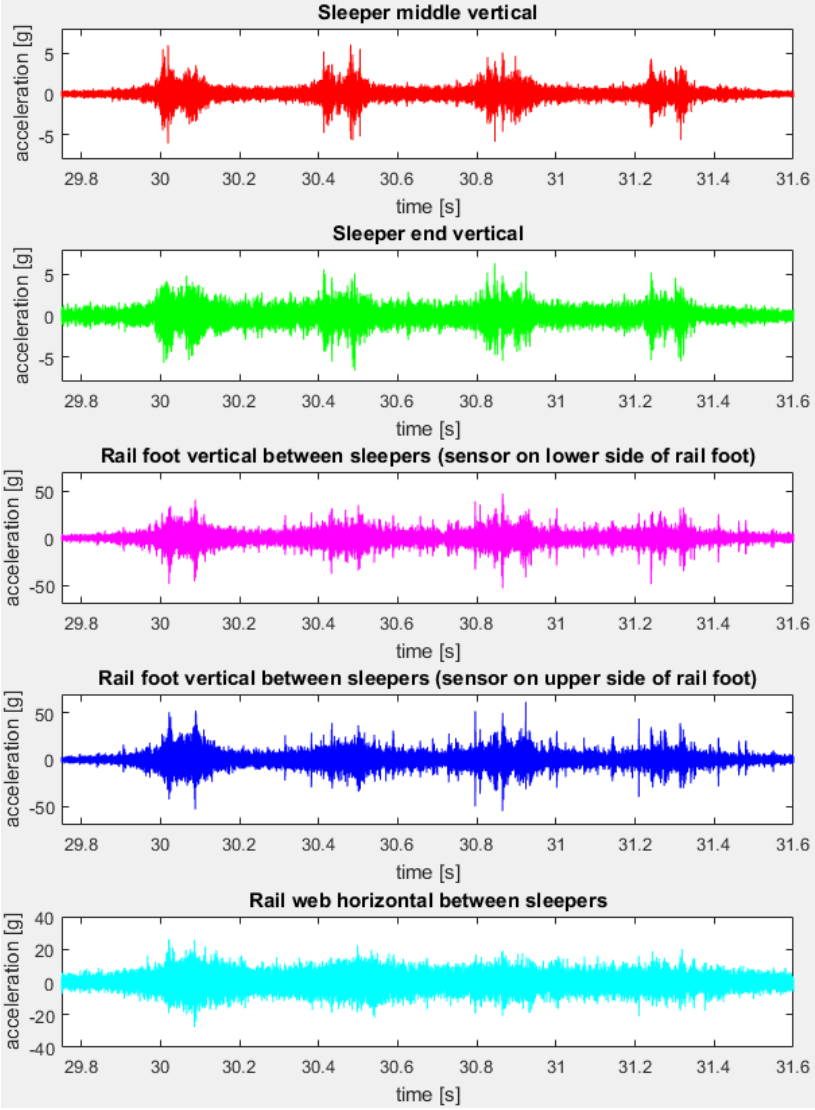

Figure 30 Reference (TUM) records from train passage 4

Figure 31 shows the acceleration data recorded by the DESTinationRAIL sensors. Vertical acceleration on the rail web overleaped sensor g-range, therefore the output went into the saturation as shown in Figure 31. Measurement on the sleeper recorded signals within the range for all three axes.

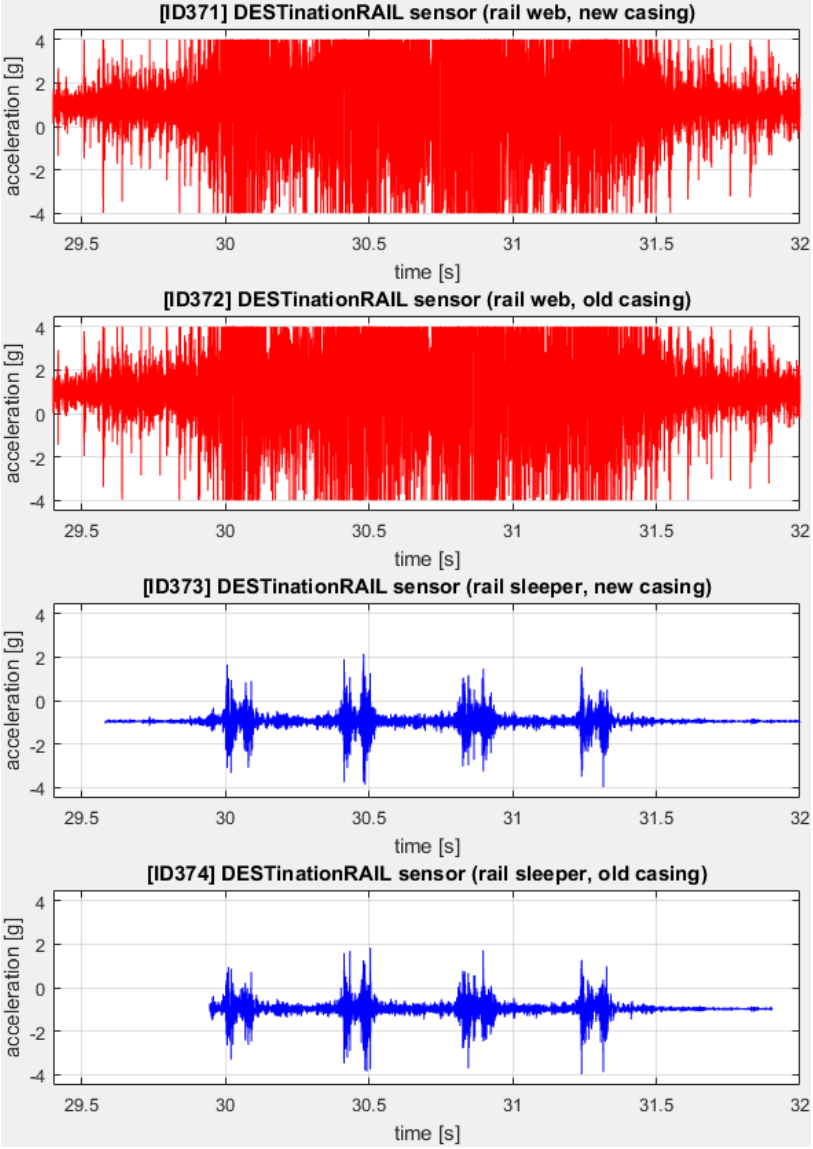

Figure 31 DestinationRAIL records from train passage 4

Figure 32 shows in detail all three axes and their acceleration signals. The vertical axis went into the saturation for the rail web sensor, lateral and longitude axis recorded usable signal within the range. The vertical, longitudinal and lateral accelerations measured at the middle of the sleeper are within the accelerometer range and signal stood unsaturated. This was same for all the train passes.

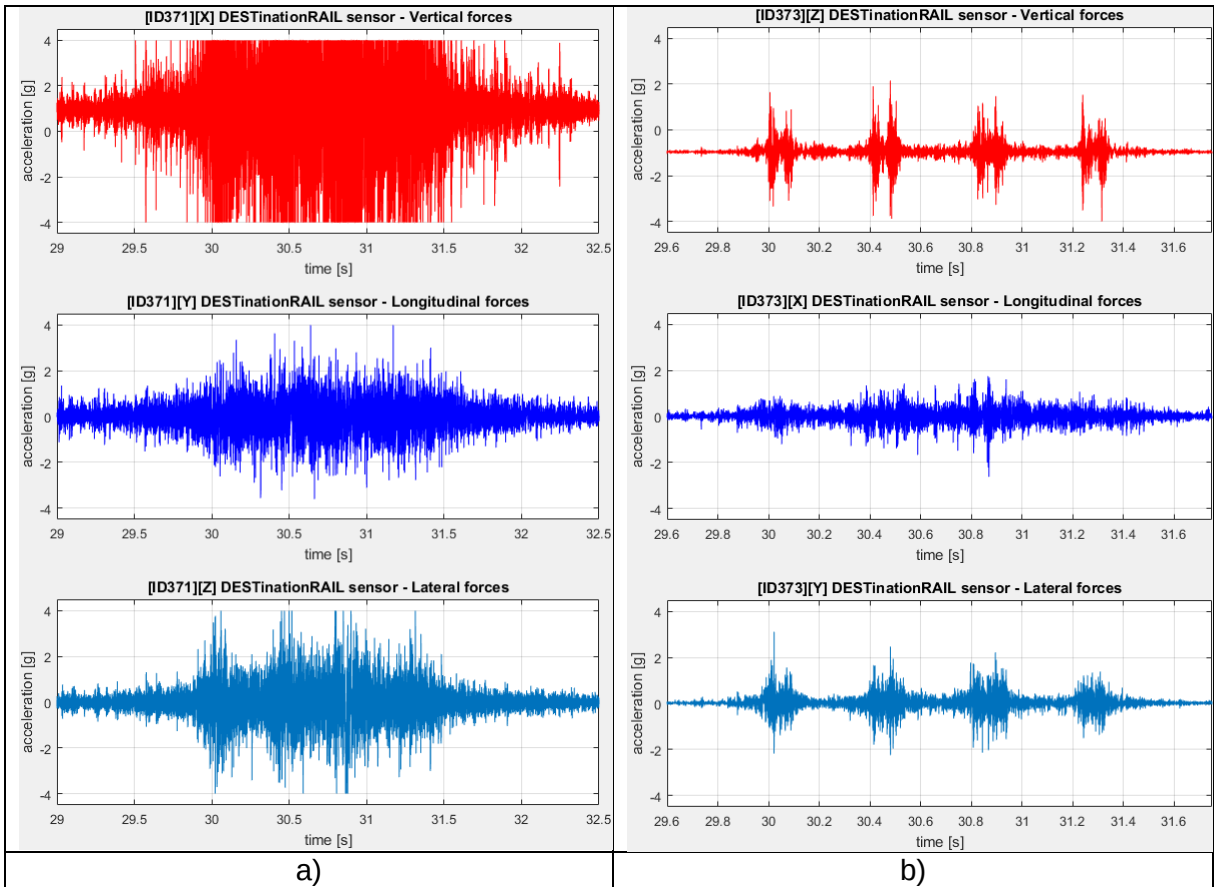

Figure 32 Acceleration records of train passage 4 by DestinationRAIL sensor: (a) at the rail web with new casing, and (b) at the middle of sleeper with new casing

The reference sensors were sampling on 25,6 kHz, so they contain 8 times more data than DESTinationRAIL sensors that were sampling just on 3,2kHz. For comparison purposes, DESTinationRAIL sensor data were overlaid over the reference data (without any down-sampling), Figure 33. Therefore, reference sensors sometimes captured the acceleration peaks at moments, when the DESTinationRAIL sensors were not sampling. Figure 34 shows the signal measured at the sleeper by the reference TUM sensor and the DESTinationRAIL sensor.

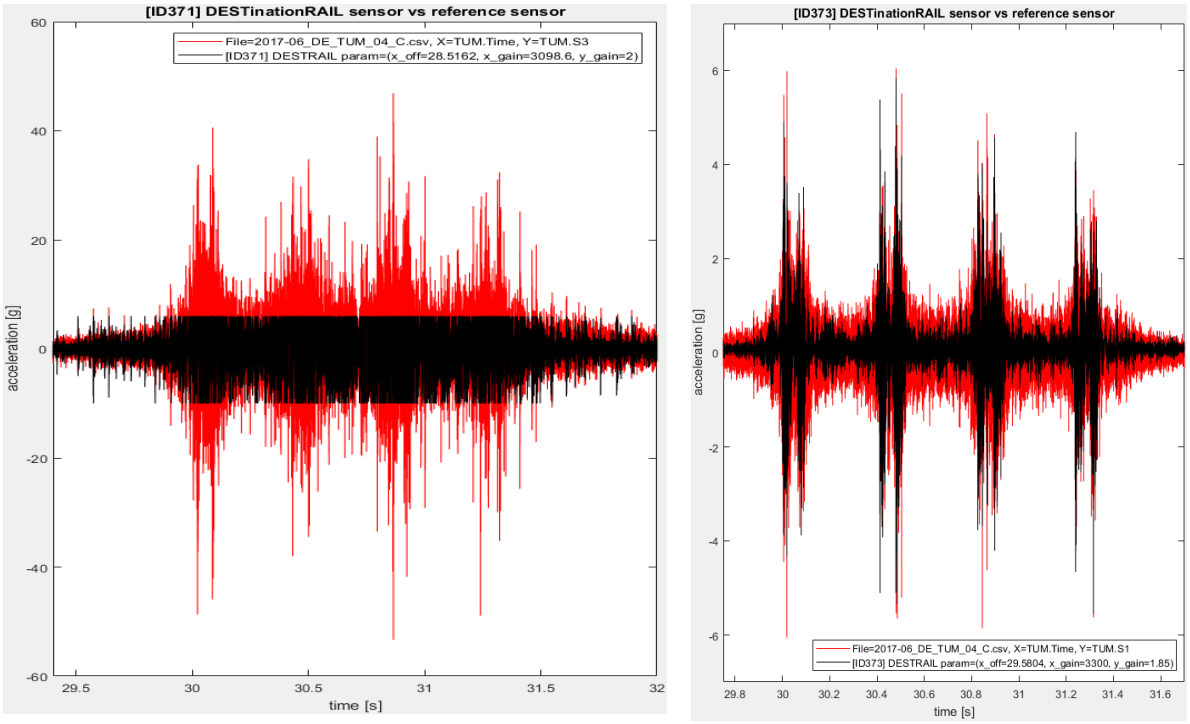

a) b)

Figure 33 Comparison with reference sensor for train passage 4: (a) sensor at the rail web with new casing, and (b) sensor at the middle of sleeper with new casing

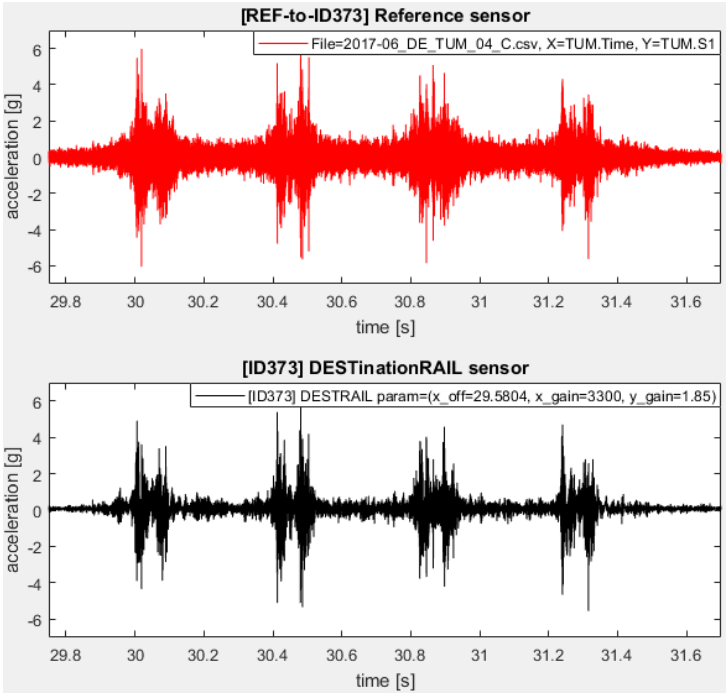

Figure 34 Acceleration measured at the middle of the sleeper using: (top) reference sensor (TUM), (bottom) DESTinationRAIL sensor

5.4.2.2 Measuring abnormal events

During the test day several train passes were measured. Some of the abnormal events from few train passes with possible defects were also detected by the measured signal. Figure 35 shows the normal (healthy) train pass with distinct peaks for all axle passes. Figure 36 shows for two trains suspected with fault. This was possible to notice during the test from the noise and vibration of these two specific train passes. These two specific trains (or one train passing twice) have either some defects on the wheels or in the suspensions.

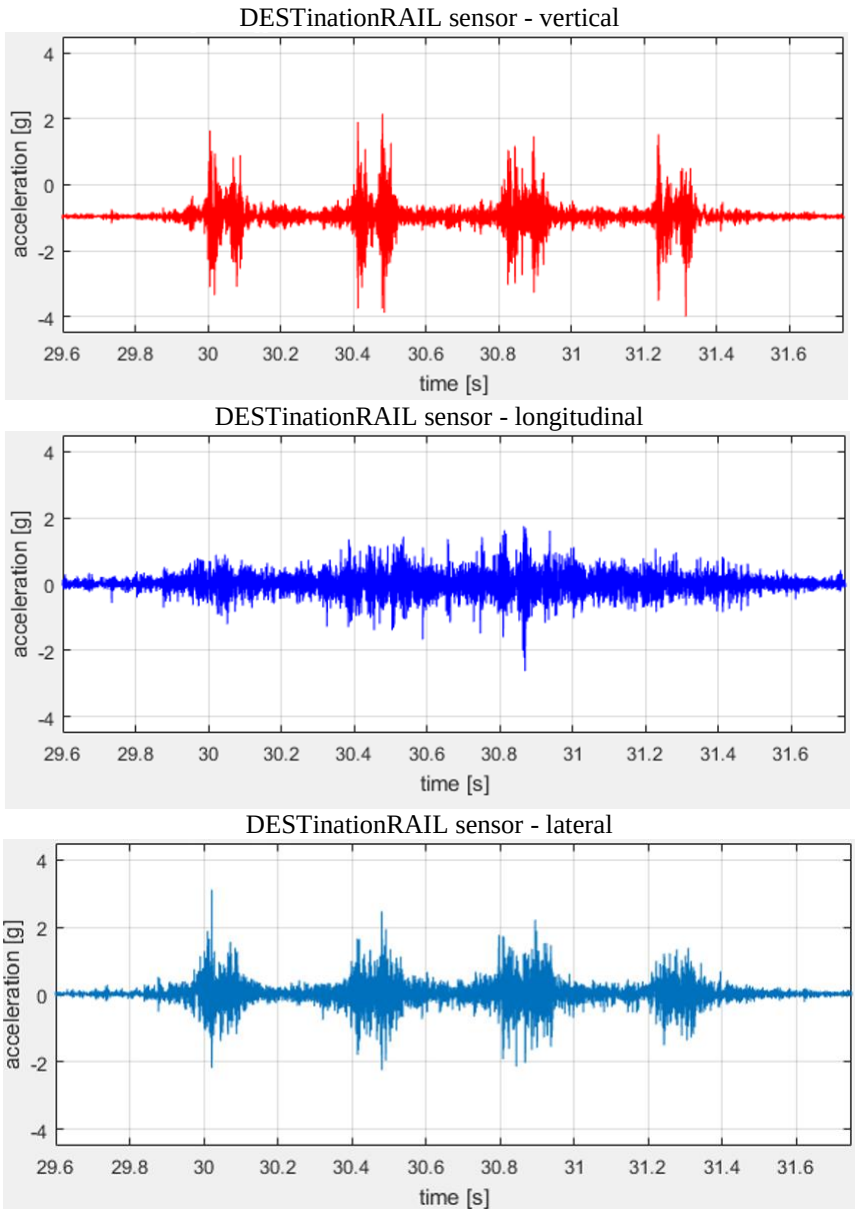

Figure 35 Acceleration measured at the middle of the sleeper for a healthy train pass

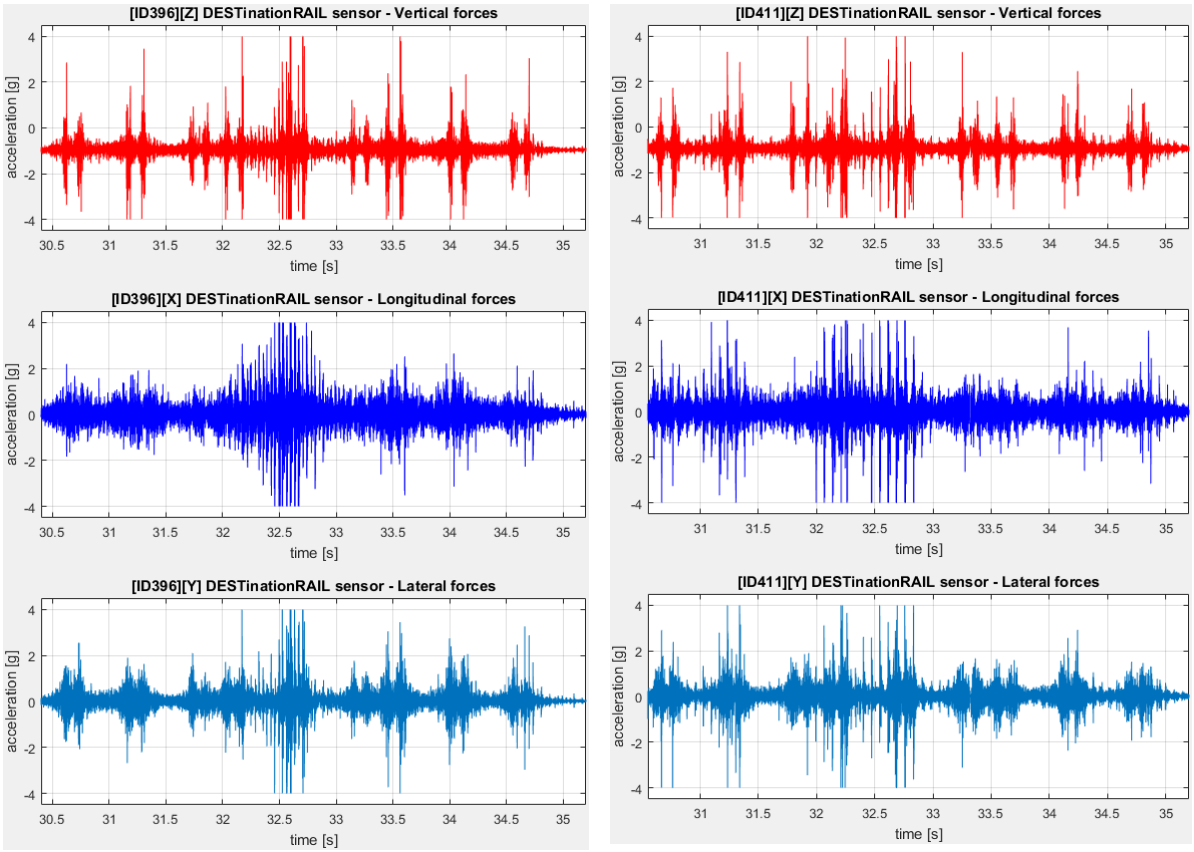

a) b)

Figure 36 Acceleration measured at the middle of the sleeper for: (a) faulty train 1, and (b) faulty train 2

6 Conclusions

This report introduced affordable low-cost technology for continuous monitoring of critical track infrastructure such as switches and crossings. Moreover, the system is able to be deployed to gather other telemetry from various sensors along the rail as well. The structure can be easily extended by another type of sensors allowing e.g. monitoring of landslides, train telemetry or any other low-amount type of data traffic.

Vehicle-track-substructure model

A vehicle-track-substructure dynamic model was developed by integrating an MBS code Gensys and an FE tool Abaqus. The vibration acceleration of rail structure under the passing train was studied for ballasted track. From the numerical results obtained, the following conclusions are drawn.

i. The wheel-rail impact is directly on the railhead; hence, the acceleration of railhead is maximum in comparison to that of rail web and rail foot. In the section between sleepers, the acceleration at the field side (outside point) on rail foot is larger than that of trackside (inside point) on rail foot. With the increase of train speed and track irregularity, the wheel-rail impact increases sharply and the acceleration of the railhead increases obviously.
ii. The rail vibration accelerations increase with the increase of the train speed. For the ballasted track where the operation speed is increased from 100km/h to 160km/h, the accelerations of railhead increased from 740 m/s^2 to 1000 m/s^2.
iii. The railhead is relatively sensitive to several effects than other positions. However, for monitoring, it requires high frequency and larger range for the acceleration sensors. In addition, it may not be possible to practically install sensors close to the railhead. Hence, the acceleration sensors should be installed at the rail web and rail foot with a marginal range of acceleration sensors.

Sensor network

Breakdown network is based on 6LoWPAN, however, due to specifics of the application it incorporates higher communication range and higher data-rates (6LoWLAN, up to ~500m, up to ~500kbps). In general, network consists of sensors (wireless sensor), gateway and cloud (WCMS). System is very scalable and may be easily integrated into GSM-R network (ERTMS) by switching the GSM modem for GSM-R version. To ensure, that the gateway is in accordance with the legislation, the whole gateway was tested in an antenna lab. During this the crucial parameters were set and validated against reference antenna in the controlled environment.

It was also found that both sensor casings (old and new) are dumping the acceleration by factor 2 without any noticeable deformations in the plot. Therefore, the current ±4g

sensor can be used for measuring higher accelerations up to about ±8g. The sensors performed very well on the sleeper where 100% of the signals recorded were within the range. From recorded data, there's no significant or visible difference between new and old casing regarding the data collecting.

The biggest drawback was saturation of the sensor attached to the rail web. Either the sensor become overloaded and didn't record any usable data or the sensors recorded data that were saturated on the vertical axis and within the range for longitude and lateral axes. For future deployment of accelerometers on the rail, replacing the sensor with higher range is suggested. The other drawback was problem with desynchronization when the signals were compared against the records of the reference one. DESTinationRAIL sensor has less precise clock and therefore produced more or less than ideal 3200 samples per second. This should be subject for a future work.

Features

The whole structure (sensors, gateway, cloud) can be remotely updated over the network. This allows to improve sensor features and functionality over the time and address any safety issue that may rise up. The second key feature is power consumption self-monitoring. Wireless sensors and gateway are capable to measure their own power-consumption to enable to determine how much energy was spent and to estimate how much battery is left. Wireless sensors and gateway are equipped by accelerometer and by temperature sensor. This allows to measure the condition of the track but might be used as well for detection of vandalism or recognizing attempt to steal the equipment.

Lifespan

The average power consumption of wireless sensor depends predominantly on amount of transferred data. If all acceleration data will be transmitted to the cloud, the estimated lifespan is about few years with respect to number of train passes per day. In case the data processing would be done locally and just status data would be transferred to the cloud, lifespan would rise up rapidly for more than a decade.

In conclusion, the system works and produce interesting results. Hence, the development of the sensors and its transmission network should continue for this and other track infrastructure applications.

7 References

[1] Persson, I, “Documentation of GENSYS. DE solver”, Östersund, Sweden, 2000.

[2] Hibbitt, Karlsson, Sorensen, “ABAQUS/Explicit (version 6.13) User's Manual”, Providence, RI, 2013.

[3] Remington, P J, “Wheel/rail rolling noise, II: Validation of the theory”, The Journal of the Acoustical Society of America, 81 (6), 1824-1832, 1987.

[4] Zhao C, Wang P, “Application of Polyurethane Polymer and Assistant Rails to Settling the Abnormal Vehicle-Track Dynamic Effects in Transition Zone between Ballastless and Ballasted Track”, Shock and Vibration, 2015.

[5] Bracciali A, Cascini G, “Detection of corrugation and wheelflats of railway wheels using energy and cepstrum analysis of rail acceleration”, Proceedings of the Institution of Mechanical Engineers, Part F: Journal of Rail and Rapid Transit, 211(2), 109-116, 1997.

[6] Cai X, Kassa E, “Detection of acceleration sensitive areas of rail using a dynamic analysis”, Proceedings of the 3rd International Conference on Railway Technology: Research, Development and Maintenance, 2016. 10.4203/ccp.110.275.

[7] Zhai W, He Z, Song X, “Prediction of high-speed train induced ground vibration based on train-track-ground system model”, Earthquake Engineering and Engineering Vibration, 9(4), 545-554, 2010.

[8] Diana G, Cheli F, Bruni S, et al, “Interactions between Railroad Superstructure and Railway Vehicles”, Vehicle System Dynamic, 23,75-86, 1994.

[9] Oscarsson J, “Dynamic train-track-ballast interaction with unevenly distributed track properties”, Vehicle System Dynamics, 37（Supp 1）: 385-396, 2002.

[10] Wickens A.H, “Fundamentals of rail vehicle dynamics”, SWETS & ZEITLINGER, Lisse, Netherlands, 2005.

[11] Shi J, Burrow M P N, Chan A H, et al, “Measurements and simulation of the dynamic responses of a bridge-embankment transition zone below a heavy haul railway line”, Proceedings of the Institution of Mechanical Engineers, Part F: Journal of Rail and Rapid Transit, 227(3), 254-268, 2013.

[12] Insa R, Salvador P, Inarejos J, et al, “Analysis of the influence of under sleeper pads on the railway vehicle/track dynamic interaction in transition zones”, Proceedings of the Institution of Mechanical Engineers, Part F: Journal of Rail and Rapid Transit, 0954409711430174, 2011.

[13] Barke D, Chiu W K, “Structural health monitoring in the railway industry: a review”, Structural Health Monitoring, 4(1), 81-93, 2005.

[14] Lee M L, Chiu W K, “Determination of railway vertical wheel impact magnitudes: Field trials”, Structural Health Monitoring, 6(1), 49-65, 2007.

[15] Tomas K., “Track Irregularities for High-Speed Trains”, Sweden Stockholm: KTH, 2009.

[16] http://www.analog.com/en/products/sensors/accelerometers.html

[17] Chraim F, Puttagunta S, “Monitoring Track Health Using Rail Vibration Sensors”. Academia. [Online] [Cited: 7 20, 2015.]

[18] Tsunashima H, Naganuma Y, Matsumoto A, Mizuma T and Mori H, “Condition Monitoring of Railway Track Using In-Service Vehicle”, Journal of Mechanical Systems for Transportation and Logistics, vol.3, P.154-165, 2010.

[19] IQRF TR-76D. IQRF. [Online] [Cited: 11 30, 2016.] http://www.iqrf.org/products/transceivers/tr-76d.

[20] IQRF Cloud. IQRF. [Online] [Cited: 11 30, 2016.] http://www.iqrf.org/images/iqrf-cloud-principle.jpg.

[21] World Rank Solutions. [Online] [Cited: 11 30, 2016.] http://www.worldranksolutions.com/wp-content/themes/springfield/img/Page-Images/Drupal-Web-Development.png.

Appendix A: Schematic

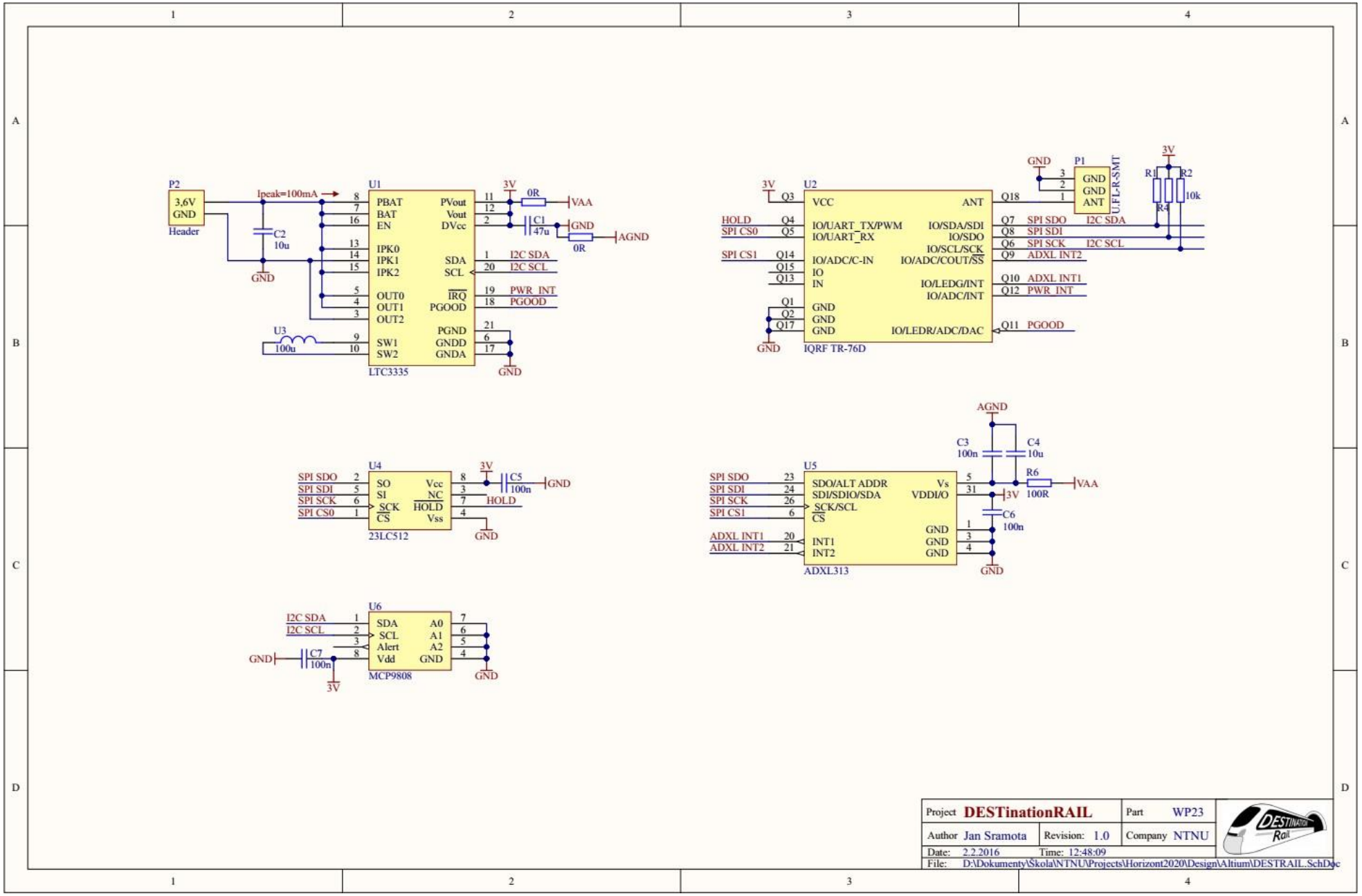

Figure A1 Schematic

Appendix B: PCB Layout

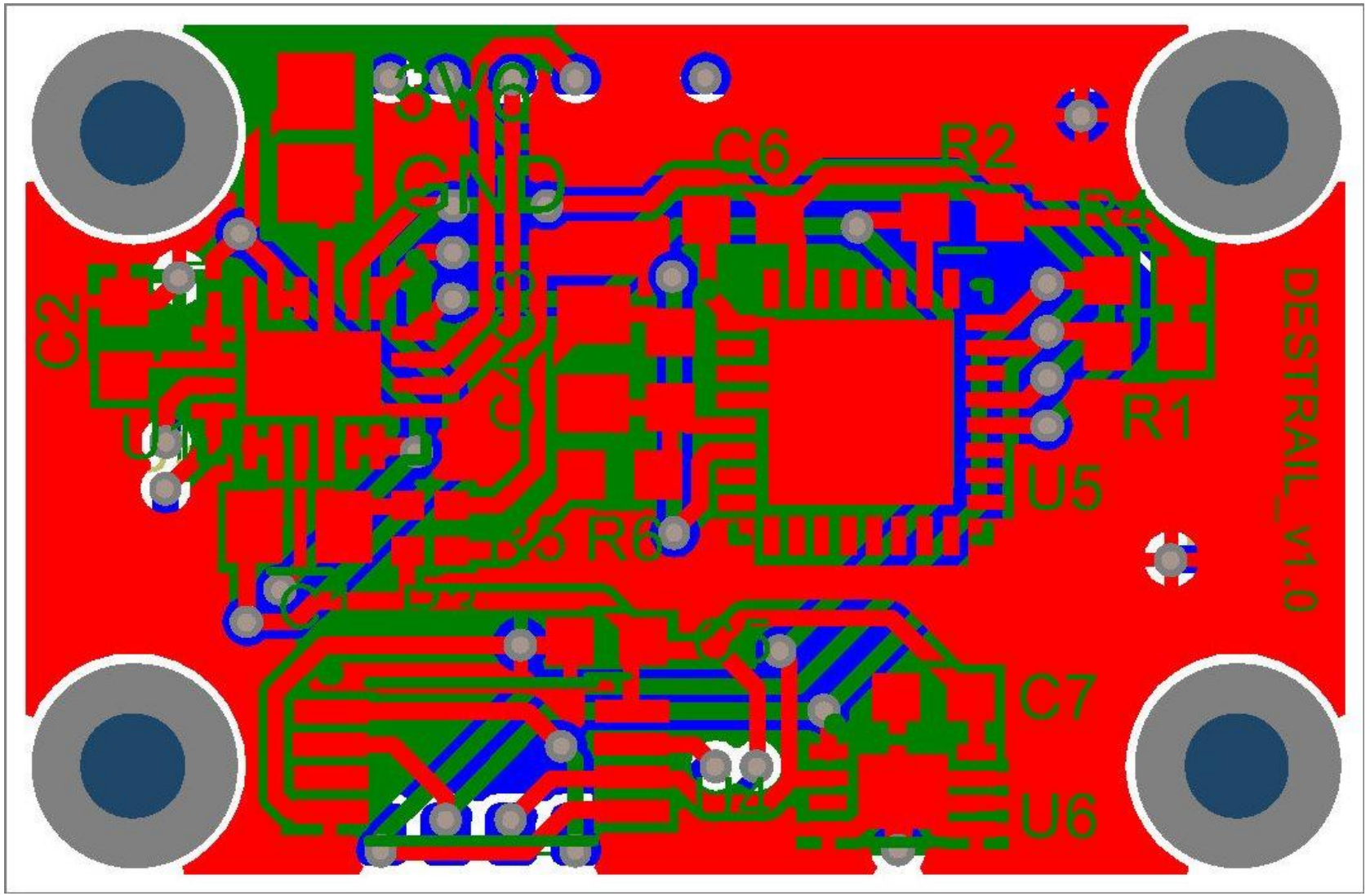

Figure B1 PCB layout

Appendix C: Tommerup Test site

Figure C1 Tommerup test site overview - switch on left, cabinet with installed gateway on right

Figure C2 Sensor on the rail web

Figure C3 Sensor on the rail web

Figure C4 Sensor on the rail web (top view)

Figure C5 Sensor on sleeper

Figure C6 Setting sensor threshold for incoming trains

Figure C7 Test passage over the wireless sensors

Appendix D: Acceleration Measurements

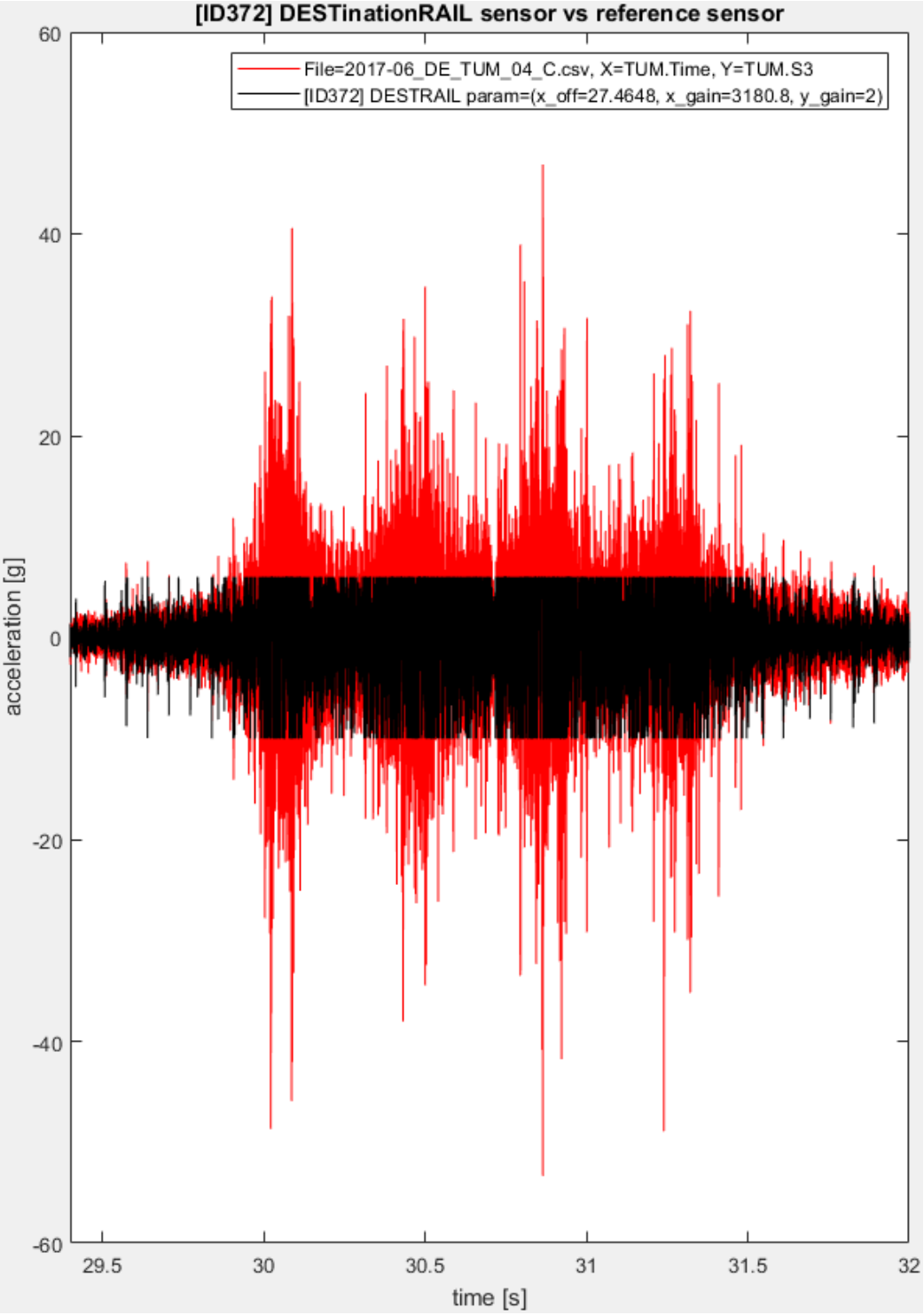

Figure D1 Acceleration signals on rail web for Train 4

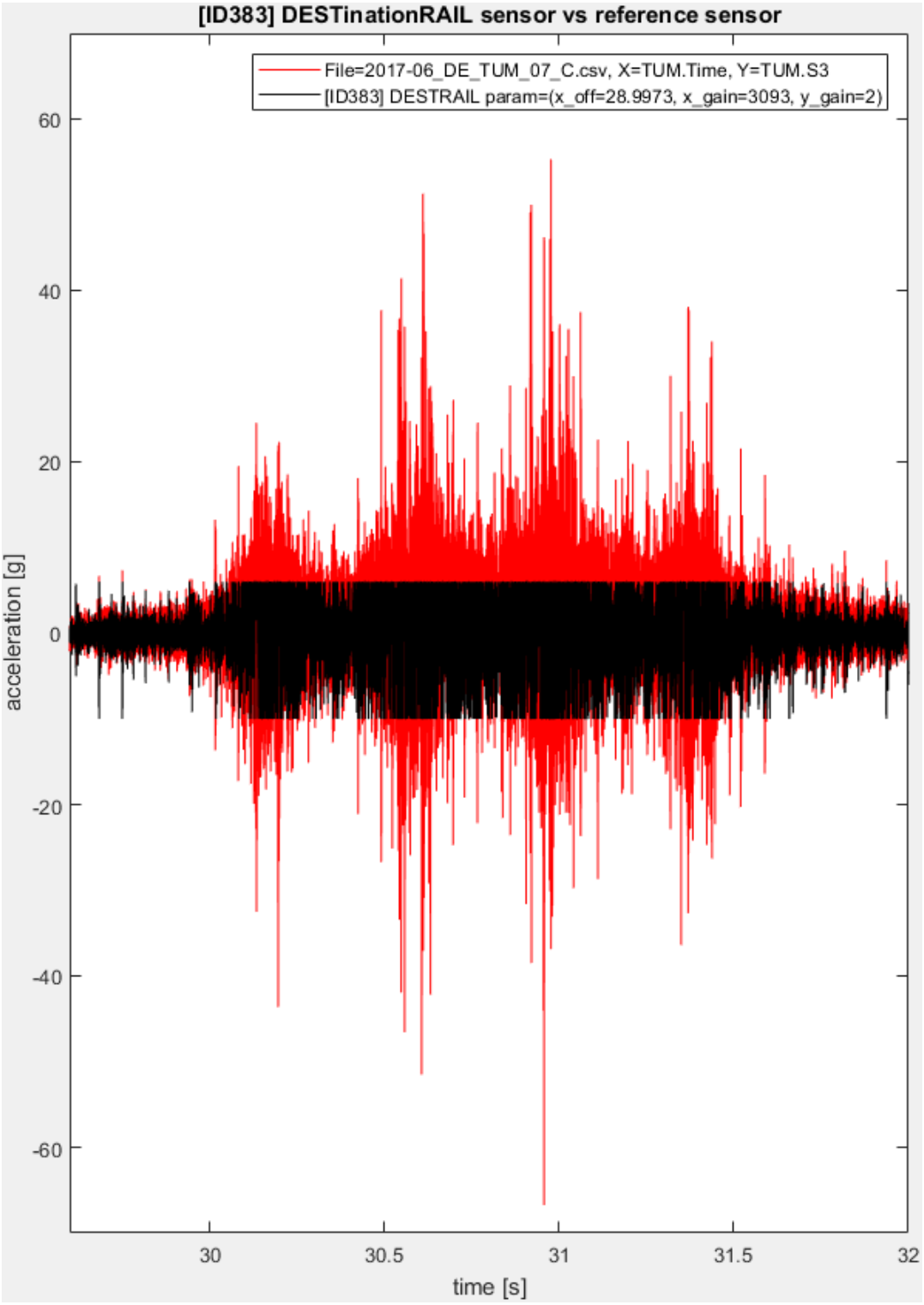

Figure D2 Acceleration signals on rail web for Train 7

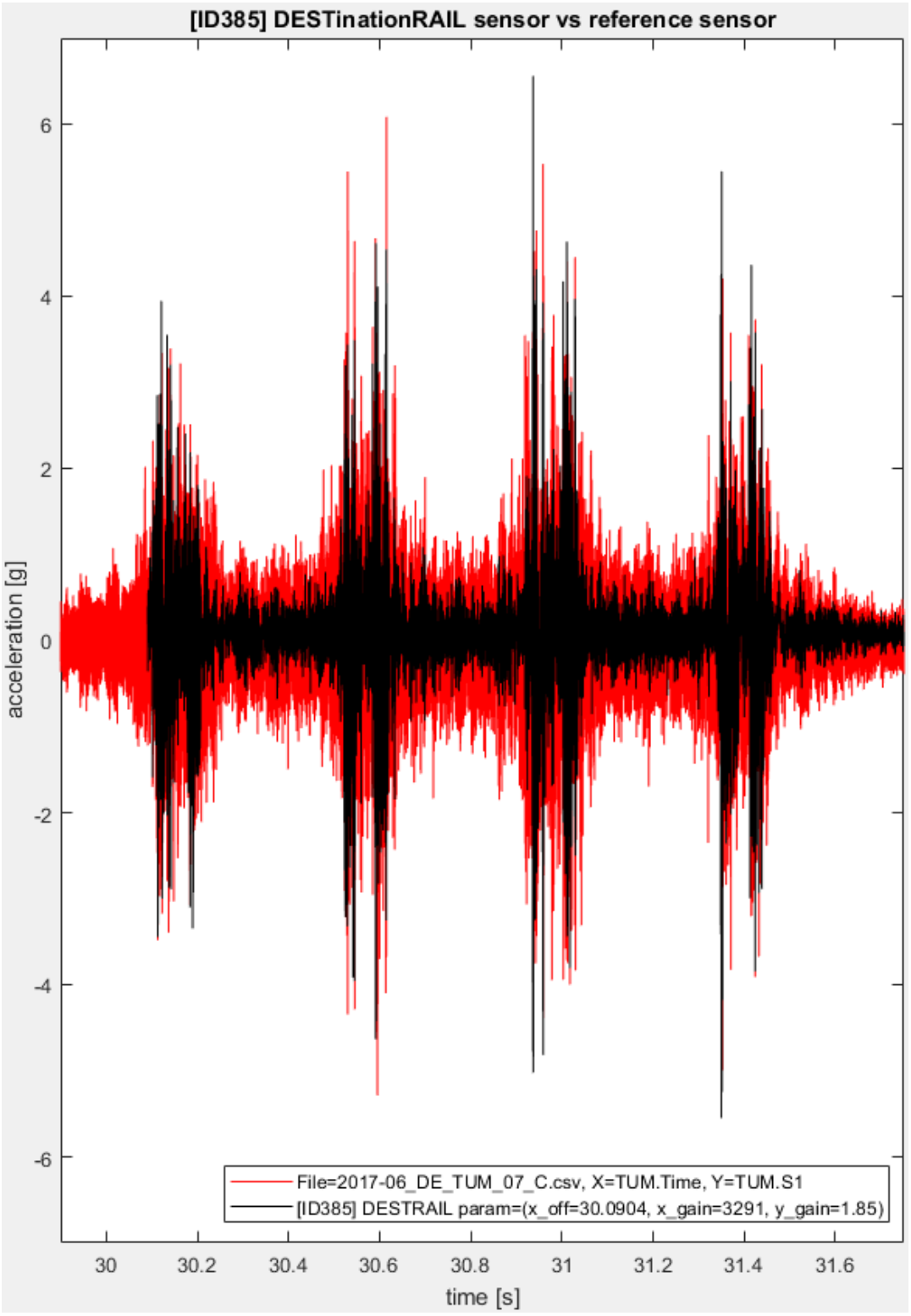

Figure D3 Acceleration signals on sleeper for Train 7

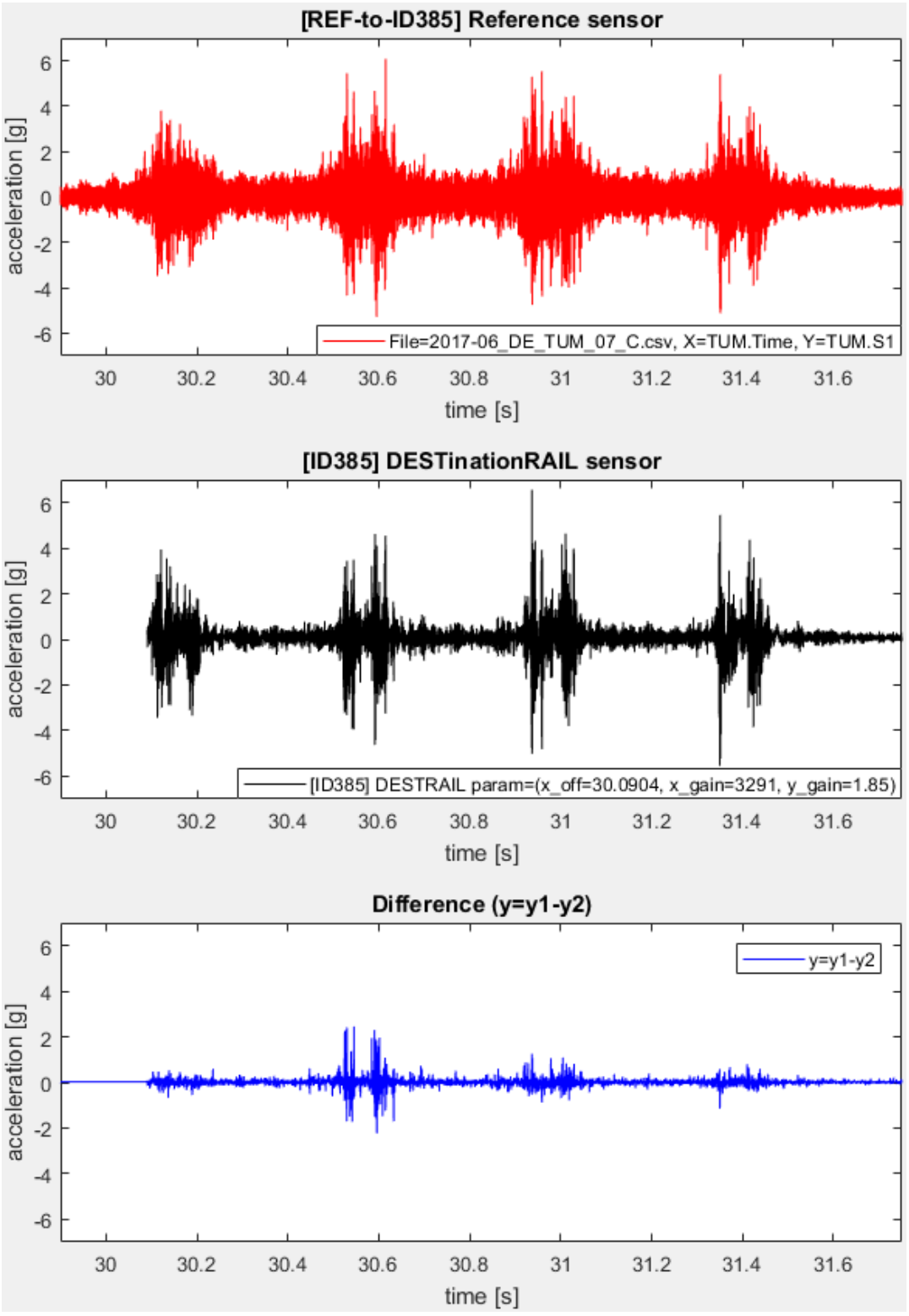

Figure D4 Difference in acceleration signals between Reference and DESTinationRail sensor with new casing on sleeper for Train 7

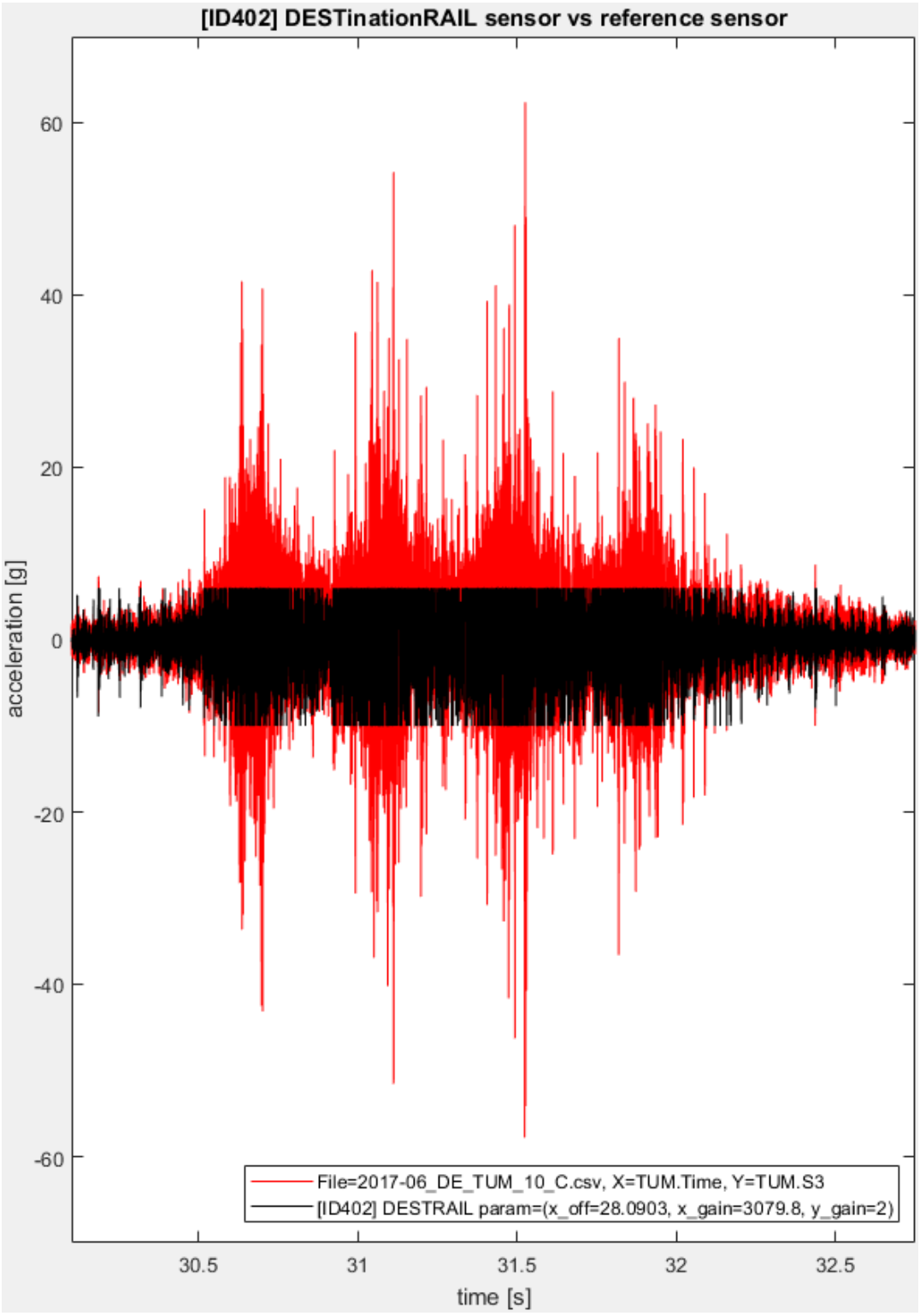

Figure D5 Acceleration signals on rail web for Train 15

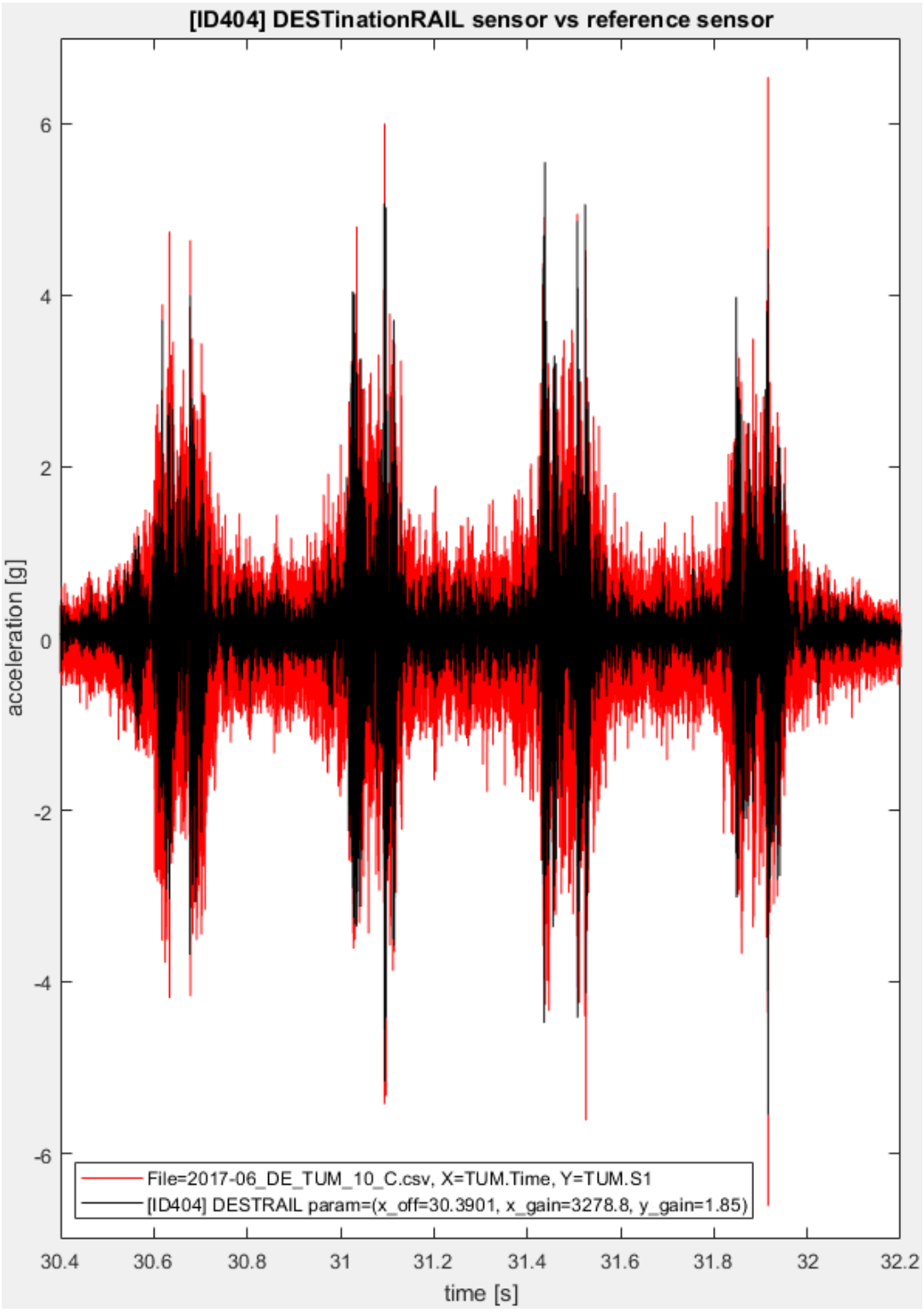

Figure D6 Acceleration signals on sleeper for Train 15

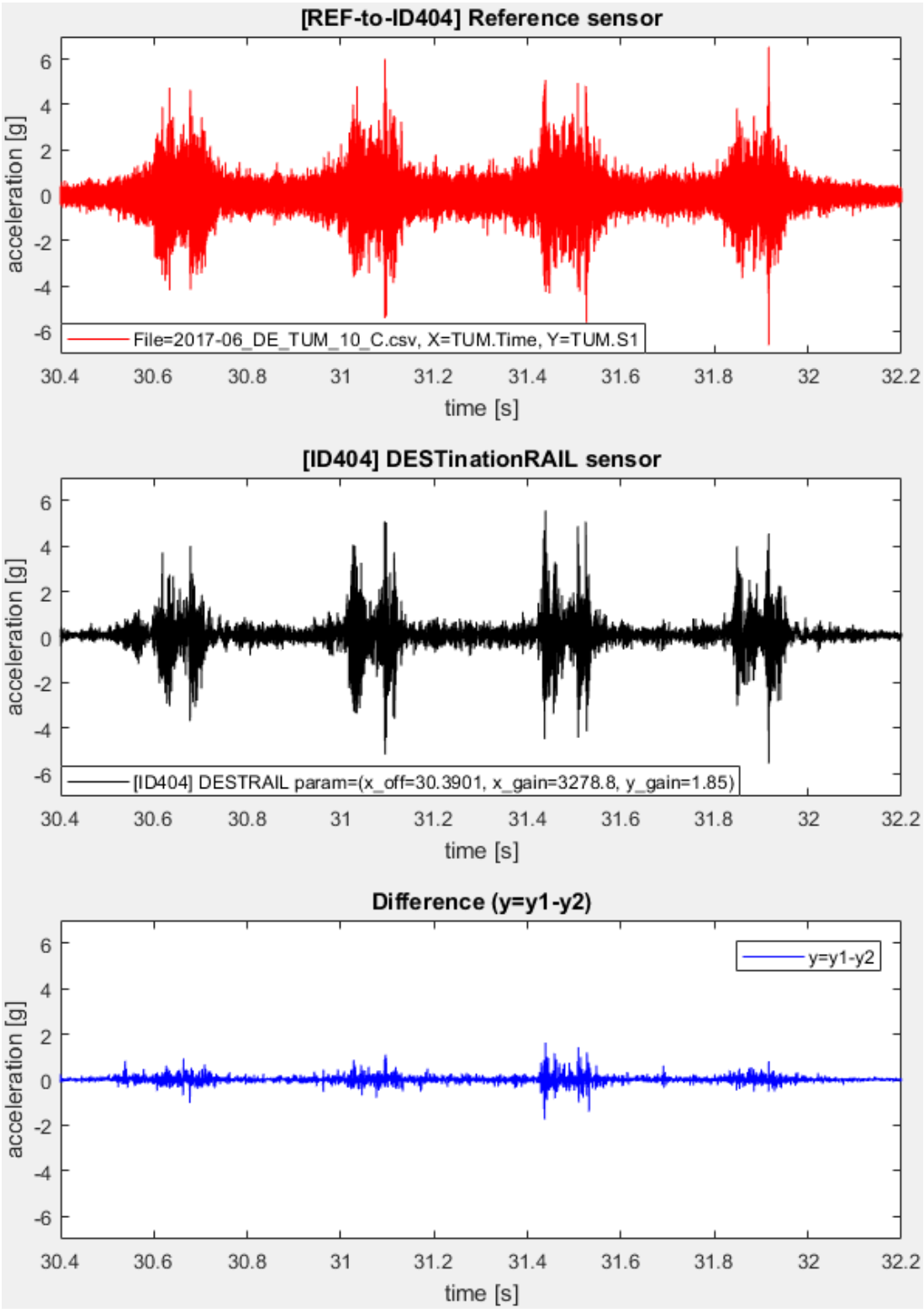

Figure D7 Difference in acceleration signals between Reference and DESTinationRail sensor with new casing on sleeper for Train 15

Appendix E: Desynchronization

Effect of desynchronization can be seen on the Figure below where the start (1) of the plot perfectly match with the reference data same as the end (3). However, in the middle (2) the Y-values are shifted in time for 500µs (max.). This is due to the fact, that the accelerometer ADXL313 generate 3200 samples per second ideally, but in reality, this value may vary. Currently there's not any information about linearity of number of samples in time at the datasheet. Therefore, Analog Devices will be contacted in this case. Possible solution would be to match number of recorded sample against more precise clock from MCU. This might be solved by software feature.

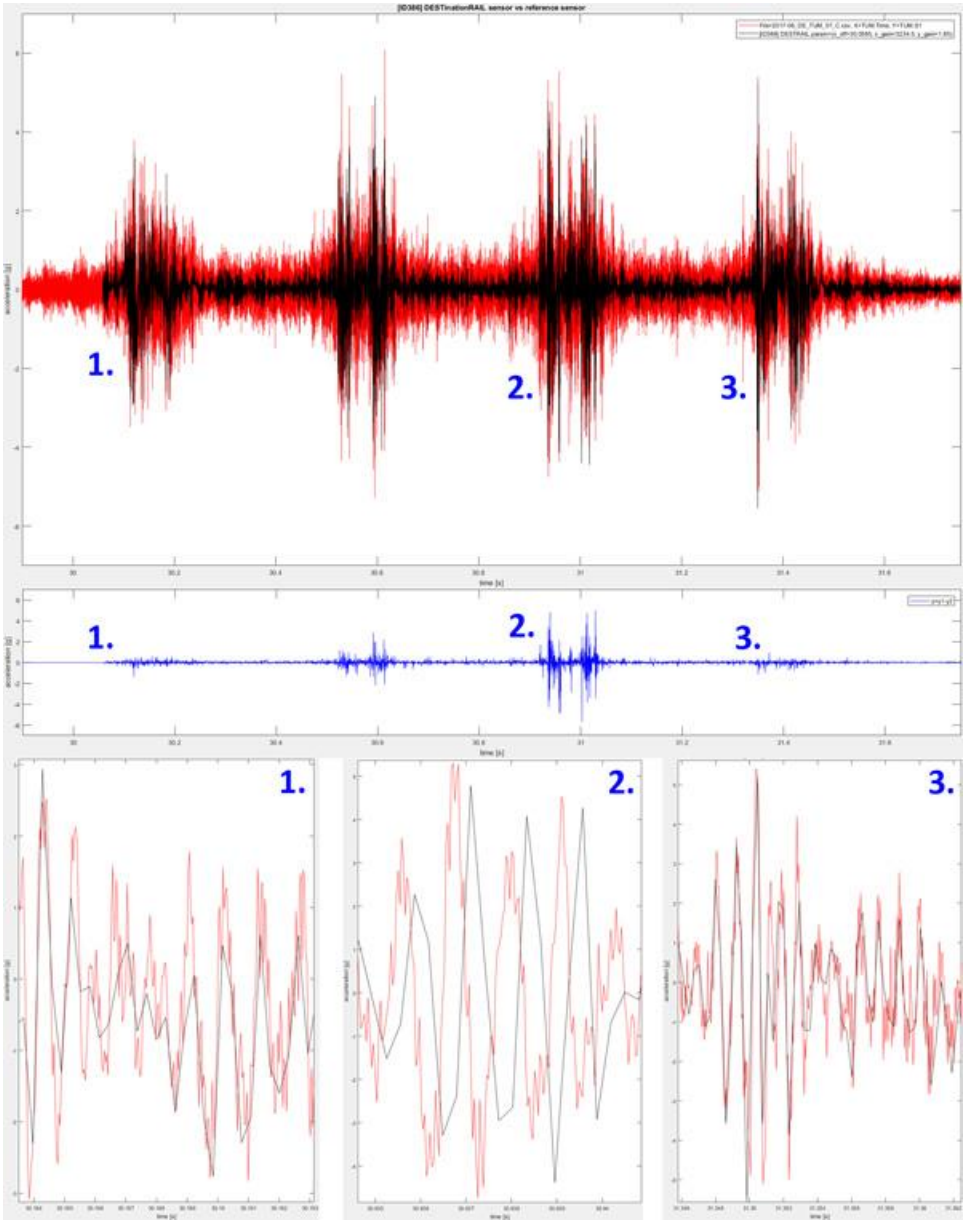

Figure E1 Example of desynchronization